Emergence and evolution of heterocyte glycolipid biosynthesis enabled specialized nitrogen fixation in cyanobacteria

Ruth Pérez Gallego[1*], F. A. Bastiaan von Meijenfeldt[1*], Nicole J. Bale[1], Jaap S. Sinninghe Damsté[1,2], and Laura Villanueva[1,2,3]

[1] NIOZ Royal Netherlands Institute for Sea Research, Department of Marine Microbiology and Biogeochemistry, PO Box 59, Den Burg 1790 AB, The Netherlands.

[2] Utrecht University, Faculty of Geosciences, Department of Earth Sciences, PO Box 80.021, Utrecht 3508 TA, The Netherlands.

[3] Utrecht University, Faculty of Sciences, Department of Biology, Utrecht 3584 CS, The Netherlands.

* These authors contributed equally to this work.

Corresponding authors: Ruth Pérez Gallego ruth.perez.gallego@nioz.nl and F. A. Bastiaan von Meijenfeldt bastiaan.von.meijenfeldt@nioz.nl.

Keywords: heterocytous cyanobacteria, nitrogen fixation, heterocyte glycolipids, lipid biosynthesis, biosynthetic gene cluster, lipid biomarkers.

Paleontological and phylogenomic observations have shed light on the evolution of cyanobacteria. Nevertheless, the emergence of heterocytes, specialized cells for nitrogen fixation, remains unclear. Heterocytes are surrounded by heterocyte glycolipids (HGs), which contribute to protection of the nitrogenase enzyme from oxygen. Here, by comprehensive HG identification and screening of HG biosynthesis genes throughout cyanobacteria, we identify HG analogs produced by specific and distantly related non-heterocytous cyanobacteria. These structurally less complex molecules probably acted as precursors of HGs, suggesting that HGs arose after a genomic reorganization and expansion of ancestral biosynthetic machinery, enabling the rise of cyanobacterial heterocytes in an increasingly oxygenated atmosphere. Subsequently, HG chemical structure evolved convergently in response to environmental pressures. Our results open a new chapter in the potential use of diagenetic products of HGs and HG analogs as fossils for reconstructing the evolution of multicellularity and division of labor in cyanobacteria.

31 Nitrogen-fixing (diazotrophic) cyanobacteria play a major role in nitrogen cycling by transforming
32 N_2 to biologically available NH_4^+ (ref. [1–4]). To overcome the inhibition by oxygen of the
33 nitrogenase enzyme responsible for nitrogen fixation, diazotrophic cyanobacteria have evolved
34 strategies that separate oxygen-sensitive nitrogen fixation from oxygen-producing
35 photosynthesis[5]. One strategy involves the confinement of the nitrogen fixation reaction to
36 heterocytes, specialized non-photosynthetic cells. Heterocytes are surrounded by a thick-walled
37 cell envelope, composed of polysaccharides and long-chain lipids with sugar headgroups called
38 heterocyte glycolipids (HGs), that limits oxygen diffusion into the cell[6].

39 HGs detected in cultures of heterocytous cyanobacteria and in the environment are structurally
40 diverse (Fig. 1a,b), spanning a variety of alkyl chain lengths (C_{26}, C_{28}, C_{30}, and C_{32}), attached to
41 different sugar headgroups (hexoses (C_6) and pentose (C_5)), with two or three keto or alcohol
42 groups at fixed positions in their alkyl chain[7–11]. 19 distinct HGs have been structurally identified
43 to date[12]. HGs are biosynthesized by polyketide synthases (PKSs) that extend and reduce a growing
44 acyl chain in successive rounds leading to the formation of a so-called aglycone (AG), which is
45 subsequently attached to a sugar headgroup (Fig. 1a,b, Supplementary Fig. 1; refs. [6,13–15]). Thus,
46 enzymatic differences between cyanobacteria may result in the production of structurally different
47 HGs, which may reflect adaptive differences in membrane impermeabilization to N_2 and
48 oxygen[9,16]. HGs can be preserved in the sedimentary record and have been used as indicators of
49 past nitrogen fixation by cyanobacteria[17], to differentiate specific families and genera of
50 heterocytous cyanobacteria as taxonomic markers[18], and to detect cyanobacterial symbionts of
51 marine diatoms[19]. Additionally, specific HGs found in the sedimentary record have been used to
52 reconstruct past surface water temperatures[20]. However, despite the relevance of HGs for nitrogen
53 fixation and their potential as biomarkers, knowledge on their structural diversity is limited

because to date, only few cyanobacterial cultures have been examined with high-resolution mass spectrometry techniques allowing for comprehensive HG identification, including those present in low abundance.

Fossil evidence and phylogenetic analyses suggest that cyanobacteria capable of heterocyte differentiation arose between 2,450 and 2,100 million years ago (Ma), around the same time and possibly simultaneously with multicellularity and nitrogen fixation[21–23]. Evolutionary pressure for an oxygen-impermeable lipid layer to shelter the nitrogenase enzyme was likely driven by the rising oxygen levels of Earth's atmosphere around 2,400 Ma[21,24]. Heterocytes have been suggested to be evolutionary related to akinetes[25], spore-like cells produced under stress conditions by some heterocytous cyanobacteria, which are also surrounded by HGs[25,26]. Here, we reconstructed the acquisition and evolution of the biosynthetic capability to produce HGs by screening ~3,600 cyanobacterial genomes and plasmids for key genes involved in HG formation and their deposition in the cell envelope of the heterocyte. We further analyzed the lipid composition of 26 heterocytous and of 2 non-heterocytous cyanobacterial cultures using high-resolution mass spectrometry to elucidate the connection between biosynthetic capability encoded by the genome and the generated biosynthetic product. Our results reveal that HG structure evolved convergently within heterocytous cyanobacteria and suggest an origin of HGs from structurally similar molecules still produced by some non-heterocytous cyanobacteria and that are not involved in nitrogen fixation nor akinete formation today.

Results and Discussion

Genomic prediction of HG biosynthesis in Cyanobacteriia

To investigate the evolution of HG biosynthesis within cyanobacteria, we searched for characteristic genetic signatures in 3,579 publicly available cyanobacterial genomes and

77 plasmids[27] and 14 newly sequenced genomes of heterocytous cyanobacteria (this study, see
78 Supplementary Tables 1-3, Supplementary Data 1 and 2) and focused our analysis on
79 photosynthetic cyanobacteria (taxonomic class *Cyanobacteriia* within the phylum
80 *Cyanobacteriota*). We screened for the genomic presence and colocalization of 19 protein-coding
81 sequences which are clustered on the genome of *Anabaena* sp. PCC 7120 (Fig. 1c, Supplementary
82 Fig. 1; refs. [13,28]), the well-studied 'model' cyanobacterium for heterocyte formation. The encoded
83 proteins are involved in the biosynthesis of HGs, and in their export across the inner membrane
84 and cell wall—leading to HG deposition in the cell envelope just outside the outer membrane and
85 beneath the polysaccharide layer (Supplementary Table 4, refs. [6,13–15,29,30]). This genomic cluster
86 has been called the '*hgl* island'[13,28] because it contains, among others, several '*hgl*' genes (Fig.
87 1c). Here, we defined *hgl* islands as gene clusters containing homologs of at least 7 of the 19
88 queried genes (Supplementary Information).

89 To validate our genomic 'island' identification approach, we evaluated our results against a subset
90 of cyanobacteria with known morphology (Supplementary Fig. 2, ref. [31]), and analyzed the
91 genomic co-occurrence of two processes taking place in heterocytes, which are both encoded by
92 genomic clusters, HG and nitrogenase biosynthesis (the latter encoded by *nif* genes,
93 Supplementary Tables 4 and 5, Supplementary Fig. 3). This benchmark confirmed that the ability
94 to make heterocytes can be confidently inferred from the genome sequence based on the presence
95 of an *hgl* island as defined here (Supplementary Information, Supplementary Table 6).

96 ***Hgl and hgl-like islands are present throughout Cyanobacteriia***

97 We investigated the presence of *hgl* islands in the context of the phylogeny of the *Cyanobacteriia*
98 based on 24 concatenated core genes (Fig. 2a). This revealed a monophyletic group that includes
99 cyanobacteria known to produce heterocytes. Although the morphology of many of the 479

100 genomes in this clade is unknown, 367 (77%) contain an *hgl* island composed of homologs of ≥10
101 of the queried genes (Fig. 1c), and almost all can fix nitrogen based on the presence of a *nif* island
102 (Fig. 2a). This confirms previous suggestions of the occurrence of a single heterocytous clade
103 within the *Cyanobacteriia*[21,31].

104 The gene composition of *hgl* islands with homologs of ≥10 genes is largely conserved, with
105 homologs of 13 out of the 19 queried genes present on ≥88% of the islands (Fig. 2b,c), and their
106 relative position fixed within the island (Supplementary Fig. 4). This indicates that evolutionary
107 conservation of genes and their location within the *hgl* island are associated with the preservation
108 of their function in heterocyte formation. Queried genes that are not conserved may be non-
109 essential for HG biosynthesis, be essential but present somewhere else on the genome (e.g. *hetI*,
110 see Supplementary Information and Supplementary Fig. 5), or their catalytic function may have
111 been replaced by unrelated genes (Supplementary Information). The identification of 13 genes that
112 are evolutionary conserved on *hgl* islands is in good agreement with previous mutagenesis studies
113 showing that 12 of the genes are essential in *Anabaena* sp. PCC 7120 for proper HG biosynthesis
114 and deposition (*hgdACB*, *hglTE*$_A$*FGDCAB*, and *all5343*; Supplementary Information,
115 Supplementary Table 4; refs. [13,32–34]).

116 Besides, the genomes of 35 out of 2,279 cyanobacteria that are not part of the heterocytous clade—
117 and are thus not expected to make heterocytes—remarkably also encode an *hgl* island by our
118 definition (Fig. 2a, Supplementary Table 7). They include unicellular cyanobacteria like
119 *Gloeocapsa* sp. PCC 7428, part of a closely related sister clade of heterocytous cyanobacteria in
120 our phylogeny (Fig. 2a), and *Gloeobacter violaceus* PCC 7421 (ref. [13]), a distantly-related
121 cyanobacterium found at the base of the *Cyanobacteriia* (Fig. 2a), which has a uniquely simple
122 life cycle and cellular composition lacking thylakoids[35,36]. Some of the non-heterocytous

123 cyanobacteria possessing an *hgl* island do not encode a *nif* island (Fig. 2a), and are thus likely non-
124 diazotrophic. Most of the *hgl* islands of non-heterocytous cyanobacteria have a more variable gene
125 composition than the *hgl* islands of heterocytous cyanobacteria, with occasional gene duplications,
126 fusions, rearrangements, and absences, and, importantly, all lack homologs of the gene *hglT* (Fig.
127 2a) encoding the glycosyltransferase (GT) that attaches the glucose headgroup to the AG in the
128 last step of HG biosynthesis (Supplementary Fig. 1). Hence, although these cyanobacteria possess
129 clusters of homologs of HG biosynthesis genes, their divergent gene composition and phylogenetic
130 position outside the heterocytous clade suggests enigmatic biosynthetic products and a function
131 unrelated to heterocyte formation.

132 Our genomic screening also revealed that 259 of the 494 *Cyanobacteriia* that have an *hgl* island
133 possess two or more *hgl* islands (Fig. 2a,b). Many of the cyanobacteria with multiple islands
134 encode an island with a highly conserved gene composition, containing homologs of only 7 HG
135 biosynthesis genes (*hgdCB* and $hglE_AFGCA$) encoded by 5 open reading frames (ORFs) (Fig. 2d),
136 thus differing from the more extended *hgl* islands with homologs of ≥10 genes discussed above
137 (cf. Fig. 2c). Additional *hgl* islands have previously been reported for four heterocytous
138 cyanobacteria[37], however our data show they occur widespread within heterocytous cyanobacteria.
139 Because its gene composition is highly conserved and more limited in size compared to the queried
140 island it may encode biosynthetic products other than HGs, and we call this island within
141 heterocytous cyanobacteria the '*hgl*-like' island hereafter. *Hgl*-like islands are absent in some
142 akinete-forming heterocytous cyanobacteria like *Anabaena variabilis* ATCC 29413, and present
143 as the only island in a few cyanobacteria within the heterocytous clade which have lost the ability
144 to form heterocytes like *Raphidiopsis brookii* D9 (refs. [23,38]), suggesting that the biosynthetic

145 products of *hgl*-like islands are not involved in akinete nor heterocyte formation (Supplementary
146 Information).

147 Hence, our results demonstrate that HG biosynthesis genes are conserved within a monophyletic
148 heterocytous clade in *Cyanobacteriia* as a cluster resembling the *Anabaena* sp. PCC 7120 *hgl*
149 island. However, several distantly related non-heterocytous cyanobacteria also encode *hgl* islands
150 with a more divergent gene composition, and various heterocytous cyanobacteria encode an
151 additional '*hgl*-like' island, providing genomic evidence to elucidate the origin of HGs in
152 *Cyanobacteriia*.

153 ***Heterocytous cyanobacteria produce a wide diversity of new HGs***

154 To characterize the structural diversity of HGs produced by heterocytous cyanobacteria, we carried
155 out the largest HG screen to date using ultra-high-performance liquid chromatography coupled
156 with multistage high-resolution mass spectrometry (UHPLC-HRMS^n). We analyzed the lipid
157 extracts of 26 cyanobacterial cultures evenly sampled throughout the heterocytous phylogeny, all
158 grown under nitrogen-limiting conditions (Figs. 2a and 3, Supplementary Fig. 6, Supplementary
159 Table 1). We screened 88 HG structures with different chain lengths, headgroups, and functional
160 groups on their alkyl chain (Supplementary Information, Supplementary Tables 8-11), 19 of which
161 were previously reported in heterocytous cyanobacteria (refs. [7,9,10,18,39,40]). This revealed the presence
162 of 30 previously unreported HGs, increasing the number of described HGs to 49 (Supplementary
163 Information, Supplementary Table 9, Supplementary Figs. 7-10). Previously, only HGs with an
164 even number of carbon atoms in their alkyl chain had been described[8,11], yet we also detect odd-
165 numbered HGs (hexose HG_{27} diol and hexose HG_{29} keto-ol) albeit in small amounts. Although
166 most HGs described thus far contain a hexose headgroup, we discovered HGs with various other
167 headgroups, including a still undetermined C_6 sugar. In addition, our broad screening reveals novel

168 chain length and headgroup combinations. The functional groups on the alkyl chain of the HGs
169 are usually diols, keto-ols, keto-diols, or triols, but we also observe novel combinations of keto
170 and alcohol groups such as diketo-ols, monofunctional HGs, and an HG with 4 functional groups.
171 The identification of these new lipids highlights the wide diversity of HGs that are produced by
172 heterocytous cyanobacteria today and opens a new avenue in the study of the role of HGs in
173 heterocyte impermeabilization and its link to nitrogen fixation.

174 ***HG structure is mostly independent of hgl island gene composition***

175 We next analyzed the distribution of HGs grouped according to their structure's characteristics—
176 headgroup, alkyl chain length, and type and number of functional groups on their alkyl chain (Fig.
177 3). Most cyanobacteria produce predominant HGs with a single combination of headgroup and
178 chain length and with 2 or 3 functional groups, and a variety of other HGs in low abundance (Fig.
179 3b). This confirms previous observations of heterocytous cyanobacteria harboring two
180 predominant HGs that are structurally identical except for differences in the number and
181 stereochemistry of keto and alcohol groups they carry[7]. For example, the two most abundant HGs
182 produced by *Chlorogloeopsis fritschii* PCC 6912 are hexose HG_{32} keto-diol and hexose HG_{32} triol
183 (this study and ref. [7]). However, others such as *Tolypothrix tenuis* PCC 7101 produce multiple
184 HGs with different headgroups, chain lengths, and number of functional groups in high abundance
185 (Fig. 3b, Supplementary Information; this study and ref. [7]).

186 No direct relationship was found between the type of HGs cyanobacteria produced and the
187 composition of their (most extended) *hgl* island, which is similar across the various species (Fig.
188 3c, Supplementary Fig. 6). Moreover, we did not find specific HGs associated with the additional
189 presence of an *hgl*-like island on the genome, further suggesting that the more compact *hgl*-like
190 islands are not involved in HG biosynthesis. The observed variation in HG distributions (Fig. 3b)

191 is thus likely due to differences in enzymatic activity of the proteins encoded by the *hgl* island (see
192 section 'HG structure evolved convergently'), available precursors, cell physiology,
193 environmental conditions, or a combination of these factors. An exception is *hglT*, the
194 glycosyltransferase (GT) that attaches the glucose headgroup to the AG (Supplementary Fig. 1),
195 which is absent from the genomes of three *Richelia* species that form symbiotic relationships with
196 marine diatoms (Supplementary Information, Supplementary Figs. 6 and 11). *Richelia*
197 *euintracellularis* HM01 and *Richelia intracellularis* RC01 both produce only HGs with a pentose
198 instead of the common hexose headgroup (Fig. 3b), which have been suggested as biomarkers for
199 diatom-diazotroph associations[9,19], and the HG profile of *Richelia rhizosoleniae* SC01 is unknown.
200 Thus, the production of pentose HGs may be directly related to the absence of *hglT* from the *hgl*
201 island, and possible replacement by an alternative GT with pentose specificity. We thoroughly
202 searched for this alternative GT on the genome of *Richelia euintracellularis* HH01 and identified
203 four candidate genes based on sequence homology to *hglT*, and functional annotation as GT
204 together with gene localization close to the *hgl* island (see Supplementary information for details).
205 However, heterologous expression of the four candidate genes in an *hglT*-deficient *Anabaena* sp.
206 PCC 7120 strain did not result in production of pentose HGs (Supplementary Information,
207 Supplementary Figs. 12-14, Supplementary Tables 12-16).

208 ***HG structure evolved convergently***

209 Next, we assessed whether the variation in HG production between cyanobacteria can be explained
210 by evolutionary relatedness, by evaluating the observed HG structural diversity in the context of
211 the core gene phylogeny (Fig. 3, Supplementary Fig. 6), which represents the evolutionary history
212 of the vertically transferred part of the genome. Since clusters of HG biosynthesis genes can be
213 horizontally transferred—as suggested by their identification on a plasmid (Supplementary

214 Information, Supplementary Fig. 2)—and may thus have a different evolutionary history, we also
215 constructed a phylogeny based on the concatenated alignment of 7 genes that are shared among
216 most *hgl* and *hgl*-like islands (Fig. 4, Supplementary Fig. 15). In this phylogeny, the most extended
217 *hgl* islands of heterocytous cyanobacteria cluster together distantly from the *hgl* islands of non-
218 heterocytous cyanobacteria and *hgl*-like islands within heterocytous cyanobacteria and have a tree
219 topology largely similar to that of the core vertically transferred genes (Fig. 5). This suggests a
220 shared evolutionary history of the core genes and *hgl* islands within heterocytous cyanobacteria
221 (Supplementary Information). The core gene and *hgl* gene phylogenies thus show similar HG
222 distribution patterns (Fig. 3 versus Supplementary Fig. 16).

223 Specific HGs are common within heterocytous subclades, such as the above discussed pentose
224 HGs of two *Richelia* species. Strains from subclades 2-4 mainly produce dominant HGs with 3
225 functional groups and even-numbered alkyl chains with ≥28 carbon atoms. Strains from subclades
226 5-9 produce primarily HG_{26}'s with 2 functional groups. However, few HGs are unique to a
227 subclade, and most HGs—especially those that are dominant in one of the cultures—are found
228 throughout the phylogeny even if in low abundance (Fig. 3, Supplementary Figs. 6 and 16). For
229 example, the pentose headgroup, which was previously detected in only a few strains, is present
230 in most cultures in relatively low abundance, although possibly in pentopyranose form
231 (Supplementary Information). Exceptions are HGs with a single functional group and odd-chained
232 HGs, which are both restricted to subclades 5-9, and pentose HG_{30} keto-triol—only found in
233 *Scytonema* sp. PCC 10023 (Supplementary Fig. 6). In addition, although cultures from closely
234 related strains usually produce similar HGs, this is not always the case. For example, *Nostoc* sp.
235 CCY 9925 and *Nostoc* sp. CCY 9926 synthesize primarily hexose HG_{28} and hexose HG_{26},
236 respectively.

237 Thus, the same HGs can be found in distantly related strains and closely related strains can differ
238 in their abundant HGs, hence challenging the common use of HGs as taxonomic biomarkers, for
239 example for members of the *Nostocaceae* and *Aphanizomenonaceae* families and for the genus
240 *Fortieaceae* (Supplementary Information, Supplementary Table 17). These findings suggest that
241 the biosynthetic process leading to HGs is flexible and can evolve convergently, i.e. independent
242 evolution of the same HG structures in different taxonomic groups (Supplementary Information),
243 possibly reflecting similar environmental pressures, leading to a chemically diverse pool of HGs
244 to accommodate them.

245 ***Hgl islands predate heterocyte formation***

246 The identification of *hgl* islands in non-heterocytous cyanobacteria and of *hgl*-like islands allowed
247 for a reconstruction of the acquisition of HG biosynthesis within the *Cyanobacteriia*. As discussed
248 above, the most extended *hgl* islands of heterocytous cyanobacteria cluster together in the
249 phylogeny based on 7 HG biosynthesis genes, as do their *hgl*-like islands (Fig. 4), and topologies
250 of both phylogenetic clusters resemble that of the core genes when a root is placed in between,
251 suggesting that a duplication that gave rise to both island types in heterocytous cyanobacteria
252 predates the Last Heterocytous Cyanobacterial Common Ancestor (LHeCCA) (Supplementary
253 Information). Phylogenetic placement of the *hgl* islands of non-heterocytous cyanobacteria—in
254 between the two heterocytous phylogenetic clusters—suggests they were not acquired via recent
255 horizontal transfer from heterocytous cyanobacteria (Fig. 4 and Supplementary Fig. 17,
256 Supplementary Table 18) and supports the presence of *hgl* islands further back in time. Given that
257 *Gloeobacter violaceus* PCC 7421 contains an *hgl* island, the duplication may predate thylakoids
258 or the last common ancestor of *Cyanobacteriia*. Alternatively, multiple horizontal transfer events
259 predating LHeCCA may have given rise to the *hgl* islands in non-heterocytous cyanobacteria

260 (Supplementary Information). In both cases, widespread loss explains the sparse distribution of
261 *hgl* islands in *Cyanobacteriia* today. Hence, the *hgl* islands in specific non-heterocytous
262 cyanobacteria likely represent a phylogenetic lineage of the island from before the emergence of
263 the heterocyte. Their diverse gene compositions suggest that this ancestral island already contained
264 many homologs of the contemporary HG biosynthesis genes—except for possibly *hglT* which is
265 absent from all non-heterocytous *hgl* islands—and reflect subsequent differential loss of individual
266 genes.

267 ***Potential origin of HGs from ancient 1,3-diols***

268 To elucidate the evolutionary origin of HG biosynthesis, we selected two cultured strains from
269 outside the heterocytous clade that contain an *hgl* island and are capable of nitrogen fixation—
270 *Pleurocapsales* cyanobacterium LEGE 10410 and *Gloeocapsopsis crepidinum* LEGE 06123 (Fig.
271 6a,b)—and exposed them to heterocyte- and akinete-inducing stresses, namely nitrogen deficiency
272 and ageing[26,41]. Microscopic analysis revealed that upon division, daughter cells of both strains
273 remain attached to the parent cell and are surrounded by a polysaccharide layer, thus appearing as
274 aggregates (Supplementary Fig. 18), under all growth conditions. Because their *hgl* islands lack
275 *hglT* homologs and contain potential ABC transporters expressed by the *hgdBC* homologs, we
276 hypothesize they can be involved in the biosynthesis and export of AGs.

277 Although no C_{26} - C_{32} HGs nor derived AGs were detected, both strains synthesize novel lipids
278 that structurally resemble canonical HGs and AGs, but with a shorter C_{24} alkyl chain and lacking
279 a characteristic functional group at the ω-1 position (Supplementary Information, Supplementary
280 Figs. 19-22). Whilst some are observed in diol form (tetracosane-1,3-diol), thus resembling AGs,
281 others consist of this same C_{24} alkyl chain compound bound to different sugars (1-(O-hexose)-3-
282 tetracosaneol, 1-(O-pentopyranose)-3-tetracosaneol, and 1-(O-dipentopyranose)-3-tetracosaneol)

283 resembling HGs (hereafter 'HG analogs') (Fig. 6c, Supplementary Tables 11, 19 and 20). We
284 speculate that these novel lipids are likely produced by the enzymes encoded by the *hgl* islands of
285 the non-heterocytous strains (Fig. 6d, Supplementary Information). Analysis of the lipid extracts
286 of the heterocytous cultures revealed that *Calothrix* sp. CCY 0018, which encodes an additional
287 *hgl* island closely related to the *hgl* island of *Pleurocapsales* cyanobacterium LEGE 10410 (Fig.
288 6b), also produces HG analogs (Supplementary Fig. 23, Supplementary Table 11), providing
289 further evidence for the biosynthesis of these lipids by an ancient phylogenetic lineage of the *hgl*
290 island (Supplementary Information).

291 As the ancestor of these islands was likely present in *Cyanobacteriia* before the emergence of the
292 heterocyte (see above), we propose that LHeCCA was already capable of synthesizing and
293 exporting C_{24} alkyl chain lipids resembling HGs and AGs for still unknown purposes
294 (Supplementary Information). Because these lipids were detected under all growth conditions
295 including in non-limited media containing nitrogen (therefore not promoting nitrogen fixation),
296 and because *hgl* islands are also present in non-diazotrophic cyanobacteria outside the
297 heterocytous clade (Fig. 2a, Supplementary Table 7) the HG analogs produced by contemporary
298 cyanobacteria, and conceivably by extension by LHeCCA, are probably not involved in nitrogen
299 fixation nor in (a process similar to) akinete formation.

300 In this scenario, the modified biosynthetic steps encoded by one of the copies of the *hgl* island of
301 LHeCCA would have allowed for the emergence of HGs from HG analogs by chain length
302 extension and the addition of new keto, alcohol, and methyl groups (Supplementary Information),
303 and facilitated their new role as nitrogenase protectors in an increasingly oxygenated atmosphere.
304 The absence of contemporary HGs with a C_{24} alkyl chain may reflect selection for longer chain

305 length potentially providing a higher oxygen impermeability to the heterocyte membrane
306 throughout the course of the evolution of heterocytous cyanobacteria.

307 Conclusions

308 The broad screening of HG composition in cultures revealed a large and previously unknown
309 structural diversity of HGs within heterocytous cyanobacteria, exposing 30 novel HGs—nearly
310 tripling known HG structural diversity. Our findings also highlight the reduced taxonomic value
311 of HGs, which complicates their use to identify their producers in present and past environments.

312 Our results support the origin of HGs from ancient HG analogs that were not involved in nitrogen
313 fixation—remnants of which may still be found in specific non-heterocytous and heterocytous
314 cyanobacteria today. Genomic clusters of HG biosynthesis genes were probably present in
315 *Cyanobacteriia* before the rise of the heterocyte. Neofunctionalization of this existing genomic
316 machinery for the production and export of 1,3-diols and related sugar-bound lipids allowed for
317 the biosynthesis of HGs and the formation of an oxygen-impermeable membrane layer to further
318 protect nitrogenase, the key enzyme for nitrogen fixation. These findings suggest the usefulness
319 of AG, HGs, and HG analogs to trace the evolution of multicellularity and division of labor in
320 cyanobacteria, which remains challenging to pinpoint due to scarcity of fossil evidence. Future
321 studies will need to evaluate the preservation potential and diagenetic transformations of these
322 molecules to fully conclude their use as fossils for molecular clock calculations of key events in
323 Earth's history and microbial evolution.

Data availability

Sequencing data and genome assemblies were deposited in the European Nucleotide Archive (ENA) under project number PRJEB67822. UHPLC-HRMS^n (Orbitrap) and GC-MS datafiles, phylogenetic trees raw files and plasmid maps can be found in supplied Supplementary Data Files and/or in the Zenodo repository https://doi.org/10.5281/zenodo.10444558.

Code availability

The code used for this manuscript is available from Zenodo at https://doi.org/10.5281/zenodo.10444558 and can be used to reconstruct all results presented here.

Acknowledgments

We thank Samuel Cirés for providing biomass of the *Umezakia ovalisporum* strains UAM 290 and UAM 292, Koichiro Awai for providing the strains *Anabaena* sp. PCC 7120 *wt* and Δ*hglT*, Michele Grego and Eveline Garritsen for assistance handling the cyanobacterial cultures, Anchelique Mets and Jessica Riekenberg for assistance during lipid extraction, Denise Dorhout and Monique Verweij for running and maintaining the UHPLC- HRMS^n analytic equipment, Marcel van der Meer for assistance on the interpretation of the GC-MS data, Judith van Bleijswijk for arranging the required permits to work with *Anabaena* sp. PCC 7120 mutants, Lora Strack van Schijndel for assistance extracting DNA from *Anabaena* sp. PCC 7120 mutants, Aniek van der Woude for helpful cloning suggestions, and Tracy Villareal and Peter C. Wolk for helpful insights on heterocytous cyanobacteria.

Funding

This work was supported by The European Research Council (ERC) under the European Union's Horizon 2020 Research and Innovation Program (grant agreement no. 694569-MICROLIPIDS) awarded to JSSD, and by the NWO-Spinoza award to JSSD. LV and JSSD received funding from

347 the Soehngen Institute for Anaerobic Microbiology (SIAM) through a Gravitation Grant
348 (024.002.002) from the Dutch Ministry of Education, Culture, and Science (OCW).

Figures

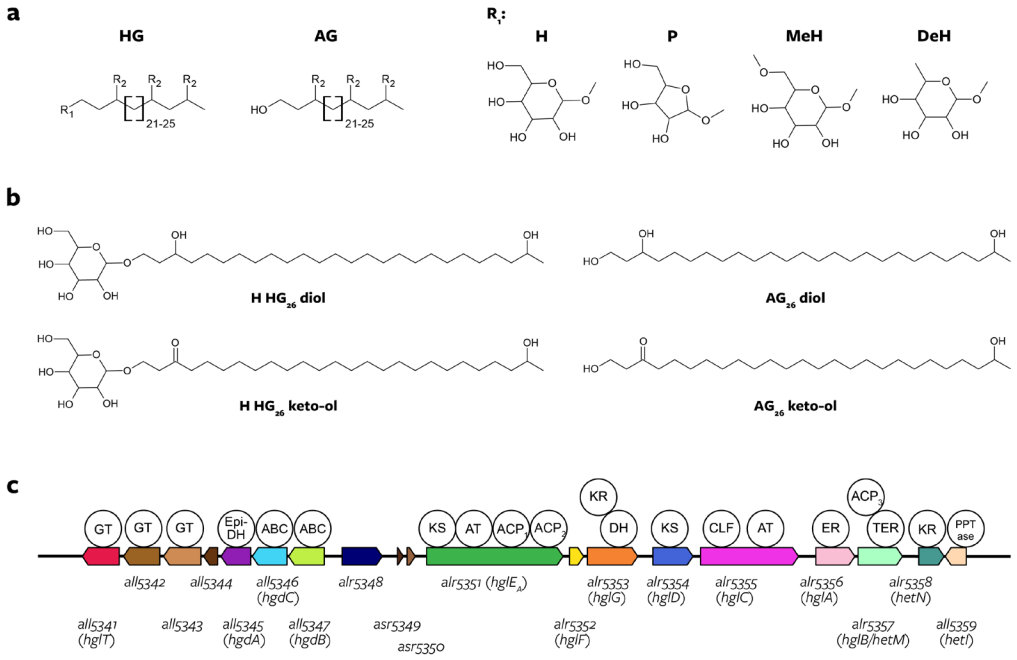

Fig. 1. Chemical structure of heterocyte glycolipids (HGs), and schematic representation of the *hgl* island of *Anabaena* sp. PCC 7120 and its most common products. a, HGs consist of a sugar headgroup that is attached to an aglycone (AG). Headgroups (R_1) are H, hexose; P, pentose; MeH, methyl hexose; and DeH, deoxyhexose. Functional groups on the alkyl chain (R_2) are H, -OH (alcohol), and =O (ketone). 19 distinct HG structures have previously been identified in heterocytous cyanobacterial cultures and in the environment (refs. [7,9,10,18,39,40]). **b**, Chemical structure of the most abundant HGs and AGs produced by *Anabaena* sp. PCC 7120. **c**, Gene cluster in *Anabaena* sp. PCC 7120 that contains genes involved in HG biosynthesis and transport (the *hgl* island). Similar clusters had also been identified in several other heterocyte-forming cyanobacteria[6,13,15]. Catalytic domains (circles) are plotted on top. Numbered genes depict the genomic naming scheme of *Anabaena* sp. PCC 7120, gene names assigned in previous publications are depicted within brackets. The known functions of *Anabaena* sp. PCC 7120 *hgl* island genes are shown in Supplementary Table 4, and the complete HG biosynthetic pathway is depicted in Supplementary Fig. 1. GT, glycosyl transferase; Epi-DH, epimerase-dehydratase; ABC, ATP-binding cassette (ABC) transporter; KS, ketoacyl synthase; AT, acyl transferase; ACP, acyl carrier protein; KR, ketoreductase; DH, dehydratase; CLF, chain length factor; ER, enoyl reductase; TER, thioester reductase; PPTase, phosphopantetheinyltransferase.

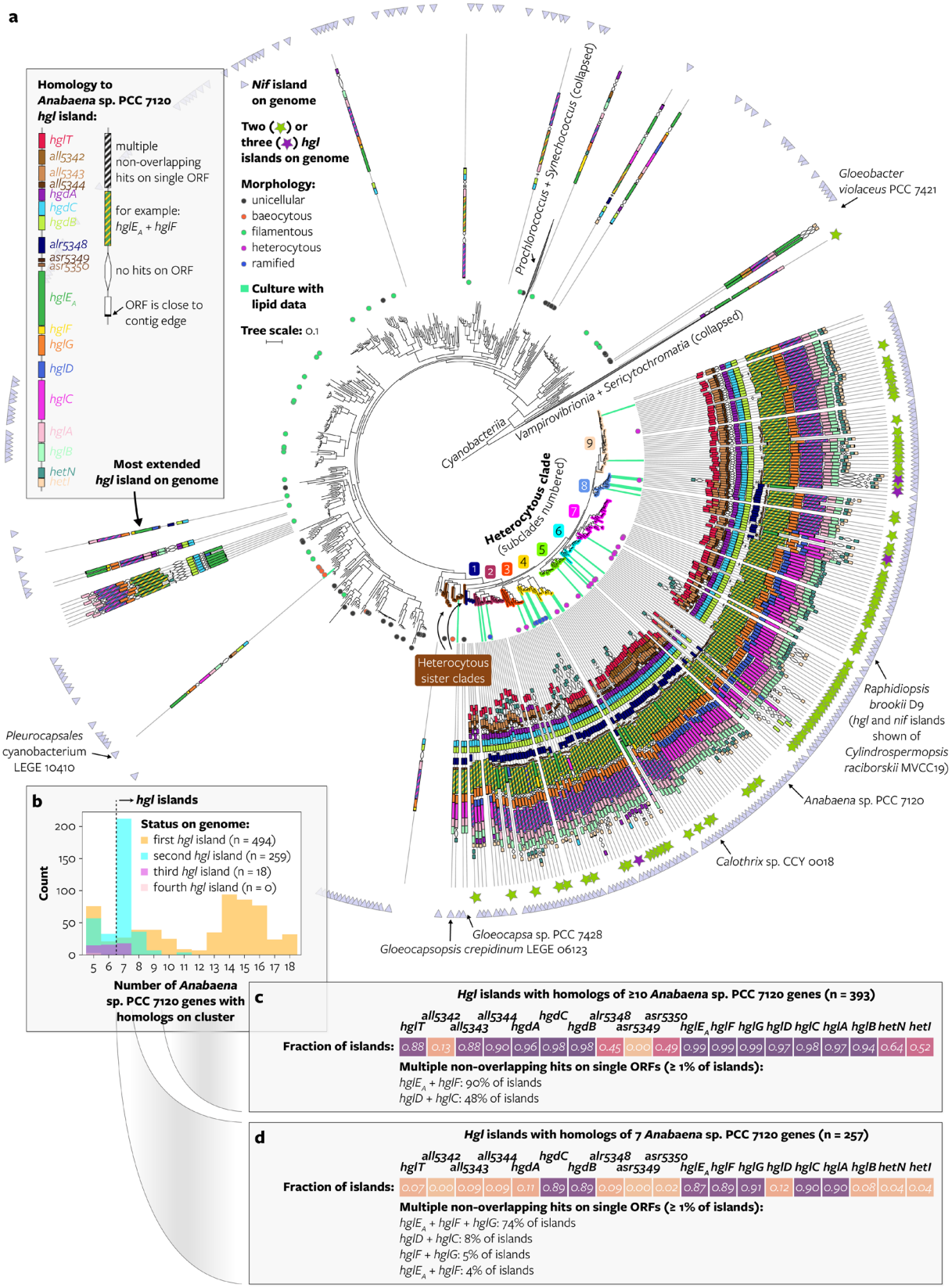
a
Homology to Anabaena sp. PCC 7120 hgl island:
hglT
all5342
all5343
all5344
hgdA
hgdC
hgdB
alr5348
asr5349
asr5350
hglE_A
hglF
hglG
hglD
hglC
hglA
hglB
hetN
hetI
multiple non-overlapping hits on single ORF
for example: hglE_A + hglF
no hits on ORF
ORF is close to contig edge
Most extended hgl island on genome
Nif island on genome
Two (✱) or three (✱) hgl islands on genome
Morphology:
unicellular
baeocytous
filamentous
heterocytous
ramified
Culture with lipid data
Tree scale: 0.1
Prochlorococcus + Synechococcus (collapsed)
Gloeobacter violaceus PCC 7421
Vampirovibrionia + Sericytochromatia (collapsed)
Cyanobacteria
Heterocytous clade
(subclades numbered)
Heterocytous sister clades
Pleurocapsales cyanobacterium LEGE 10410
Raphidiopsis brookii D9 (hgl and nif islands shown of Cylindrospermopsis raciborskii MVCC19)
Anabaena sp. PCC 7120
Calothrix sp. CCY 0018
Gloeocapsa sp. PCC 7428
Gloeocapsopsis crepidinum LEGE 06123
b
hgl islands
Status on genome:
first hgl island (n = 494)
second hgl island (n = 259)
third hgl island (n = 18)
fourth hgl island (n = 0)
Count
Number of Anabaena sp. PCC 7120 genes with homologs on cluster
c
Hgl islands with homologs of ≥10 Anabaena sp. PCC 7120 genes (n = 393)
hglT all5342 all5343 all5344 hgdA hgdC hgdB alr5348 asr5349 asr5350 hglE_A hglF hglG hglD hglC hglA hglB hetN hetI
Fraction of islands: 0.88 0.13 0.88 0.90 0.96 0.98 0.98 0.45 0.00 0.49 0.99 0.99 0.99 0.97 0.98 0.97 0.94 0.64 0.52
Multiple non-overlapping hits on single ORFs (≥ 1% of islands):
hglE_A + hglF: 90% of islands
hglD + hglC: 48% of islands
d
Hgl islands with homologs of 7 Anabaena sp. PCC 7120 genes (n = 257)
hglT all5342 all5343 all5344 hgdA hgdC hgdB alr5348 asr5349 asr5350 hglE_A hglF hglG hglD hglC hglA hglB hetN hetI
Fraction of islands: 0.07 0.00 0.09 0.09 0.11 0.89 0.89 0.09 0.00 0.02 0.87 0.89 0.91 0.12 0.90 0.90 0.08 0.04 0.04
Multiple non-overlapping hits on single ORFs (≥ 1% of islands):
hglE_A + hglF + hglG: 74% of islands
hglD + hglC: 8% of islands
hglF + hglG: 5% of islands
hglE_A + hglF: 4% of islands

Fig. 2a, Maximum likelihood cyanobacterial phylogeny created using a concatenated alignment of 24 core vertically-transferred genes[42] of 1,260 genomes representing species groups (2,758 genomes of cultured and uncultured cyanobacteria clustered at ≥95% average nucleotide identity). The tree is rooted between *Cyanobacteriia* and the non-photosynthetic *Vampirovibrionia* and *Sericytochromatia*[43,44]. Morphology of specific genomes is indicated based on ref. [31]: unicellular (grey); baeocytous (orange), strains capable of forming internal small cells (or endospores) by multiple fissions in parent cells[45]; filamentous (green), chain of cells (or trichome) without an investing sheath which grows by intercalary cell division[45,46]; heterocytous (purple) and ramified (blue) are filamentous strains that when grown in absence of combined nitrogen contain heterocytes in their trichome and that divide in one or in more than one plane, respectively[46]. HG lipid data was obtained in this study and in previous studies (Supplementary Table 1). The *hgl* and *nif* islands of one selected genome per branch are drawn on the tree (Online methods). The composition of the most extended *hgl* island in terms of number of *Anabaena* sp. PCC 7120 genes with homologs on the island is shown. For size reference, the length of the coding region of $hglE_A$ of *Anabaena* sp. PCC 7120 is 4,626 base pairs. Genomes that contain more than one *hgl* island are indicated with stars, the composition of their additional islands is not shown. The 'heterocytous clade' is defined based on the ubiquitous presence of both *hgl* and *nif* islands and contains genomes with unknown morphology. Monophyletic heterocytous subclades were manually selected. Scale bar represents the mean number of substitutions per site. ORF, open reading frame; contig, contiguous sequence. Source files in Supplementary Data 3. **b**, Size distribution of all identified gene clusters. Gene clusters are grouped according to their status in the genome, where the 'first' cluster (orange) is the most extended island in terms of number of *Anabaena* sp. PCC 7120 genes with homologs on the island, and the 'second' cluster (cyan) the second-most extended island. Sample sizes in the legend are only for *hgl* islands (here defined as genomic clusters containing homologs of ≥7 *Anabaena* sp. PCC 7120 genes). **c**, Frequency of homologs of HG biosynthesis genes on *hgl* islands containing homologs of ≥10 genes, and **d**, containing homologs of 7 genes. Color-coding in panels c and d is for legibility only and reflects the numbers within the cells, with darker colors representing a higher fraction.

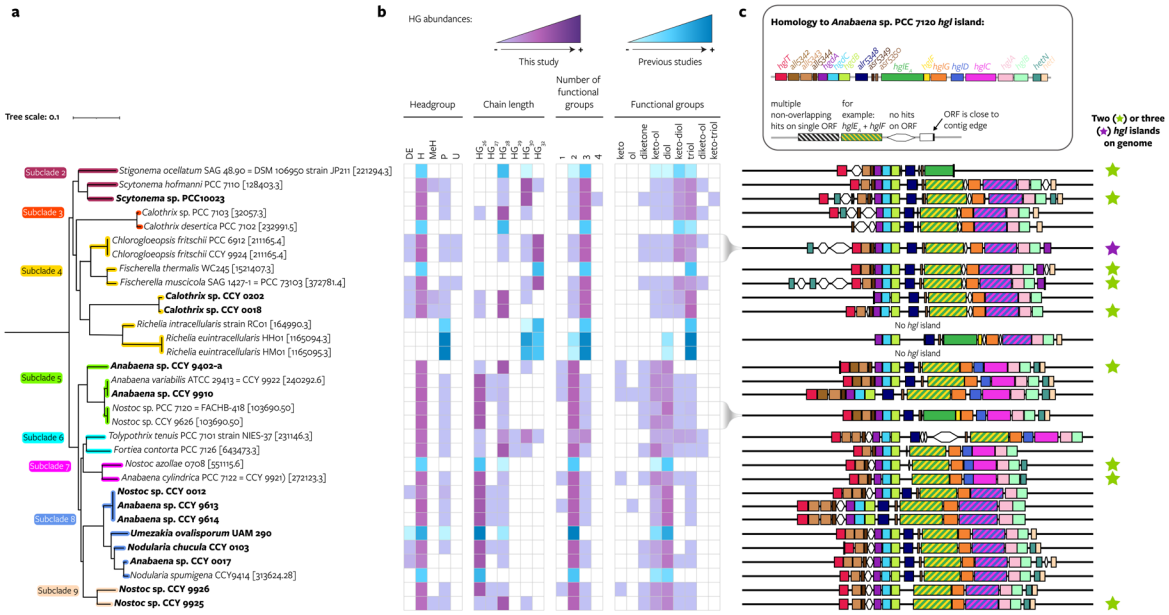

Fig. 3. Distribution of 49 HGs grouped according to their structure's characteristics throughout heterocytous *Cyanobacteriia*. a, Maximum likelihood cyanobacterial phylogeny based on 24 core vertically transferred genes including genomes with a known HG lipid profile (pruned from Fig. 2a). Genomes sequenced in this study are shown in bold. Scale bar represents the mean number of substitutions per site. **b**, Heatmap of HG relative abundances grouped according to the headgroup (H, hexose; DeH, deoxyhexose; MeH, methyl-hexose; P, pentose; U, unknown), chain length, number and type of functional groups of each HG. The same figure with all individual HGs is shown in Supplementary Fig. 6. HG abundances obtained from this study are shown in purple and those obtained from literature are shown in blue. **c**, Schematic representation of the genes present on the most extended *hgl* island on the genome in terms of number of *Anabaena* sp. PCC 7120 genes with homologs on the island**.** Stars indicate the presence of two (green) or three (purple) *hgl* islands on the genome; these additional islands are not drawn. ORF, open reading frame; contig, contiguous sequence.

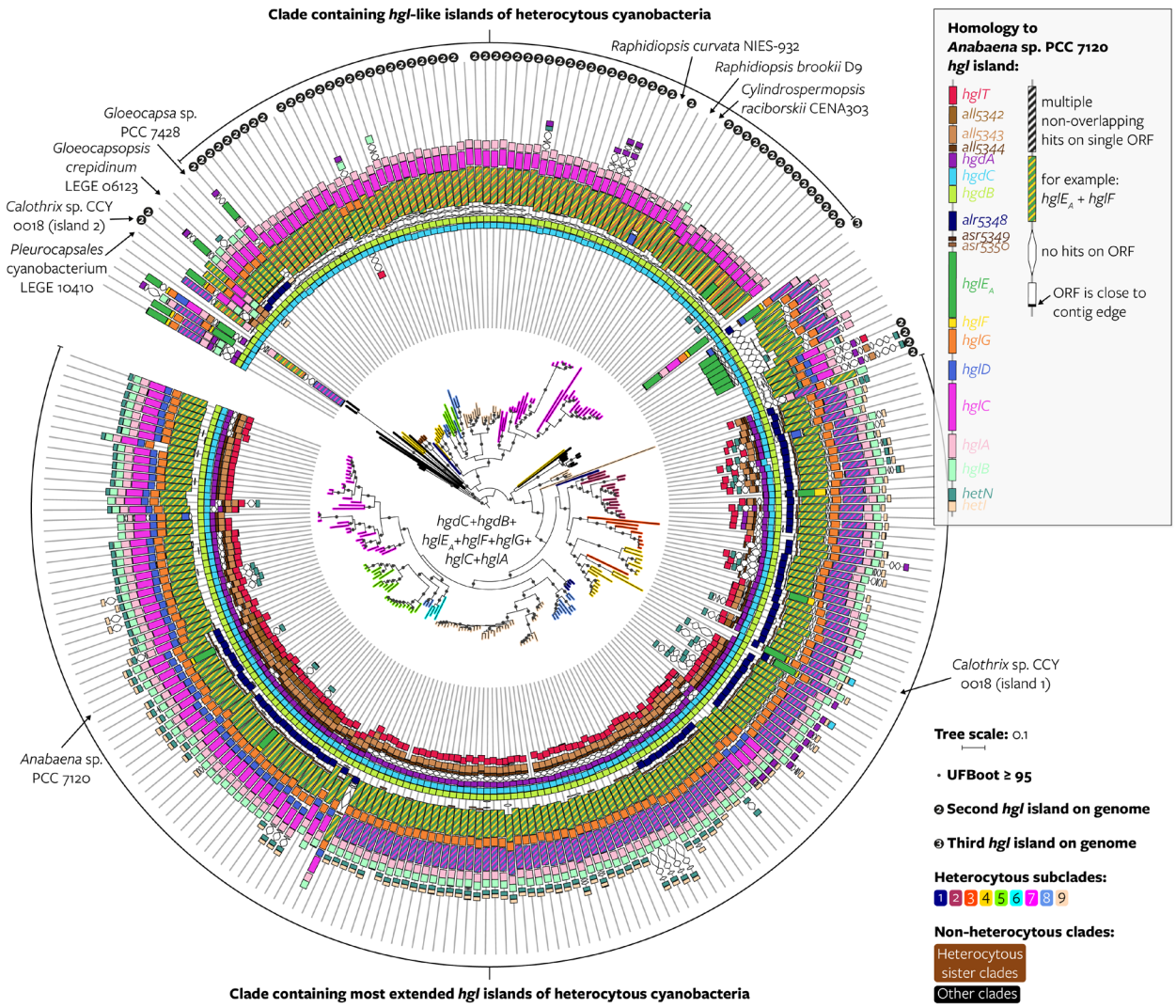

Fig. 4. Evolutionary history of *hgl* islands within *Cyanobacteriia*. Maximum likelihood phylogeny of the *hgl* island created using a concatenated alignment of homologous sequences of 7 HG biosynthesis genes (*hgdCB* and *hglE*$_A$*FGCA*) that are often present on *hgl* islands. Heterocytous and non-heterocytous subclades represent the position of the genome in the manually defined monophyletic clades of Fig. 2a based on a concatenation of 24 core vertically transferred genes. Genomes that are not part of a manually defined clade in Fig. 2a fall within the 'other clades' category in this figure. 'First', 'second', and 'third' *hgl* islands are based on the presence of other islands on the genome, where the 'first' *hgl* island (not marked) is the most extended island in terms of number of *Anabaena* sp. PCC 7120 genes with homologs on the island, the second *hgl* island (marked with a 2) the second-most extended island, and the third island (marked with 3) the third-most extended island. The *hgl*-like islands of *Raphidiopsis curvata* NIES-932, *Cylindrospermopsis raciborskii* CENA303, and *Raphidiopsis brookii* D9 are indicated because they are non-diazotrophic cyanobacteria from within the heterocytous clade. The tree is rooted at midpoint. Scale bar represents the mean number of substitutions per site. ORF, open reading frame; contig, contiguous sequence; UFBoot, ultrafast bootstrap approximation. Source files in Supplementary Data 4.

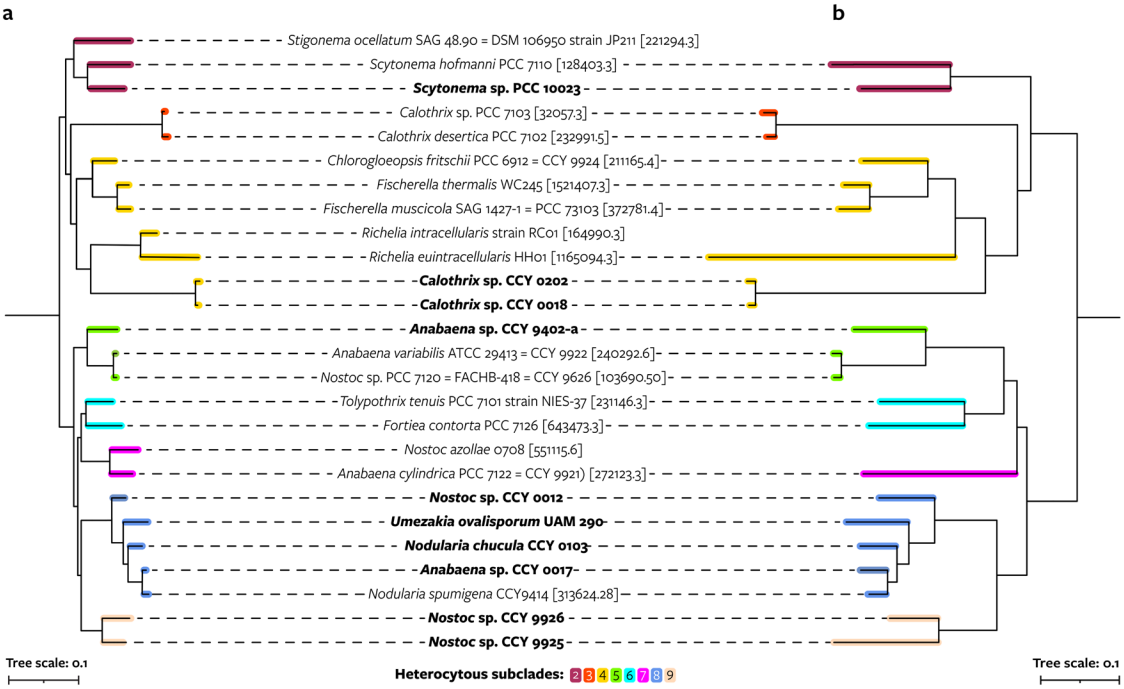

Fig. 5. Comparison between maximum likelihood phylogenies based on 24 core vertically transferred genes and 7 *hgl* island genes of genomes with a known HG profile. a, Cyanobacterial phylogeny based on 24 core vertically transferred genes (pruned from Fig. 2a). **b**, Pruned phylogeny of the *hgl* island based on homologous sequences of 7 HG biosynthesis genes (*hgdCB* and *hglE*$_A$*FGCA*) that are often present on *hgl* islands. For each cyanobacterium, only the most extended *hgl* island in terms of number of *Anabaena* sp. PCC 7120 genes with homologs on the island is shown. These *hgl* islands closely resemble the *hgl* island of *Anabaena* sp. PCC 7120 in terms of gene composition as opposed to the more compact *hgl*-like islands. The tree is rooted outside the depicted clade. Genomes sequenced in this study are shown in bold. No genomes from subclade 1 are present in the figure because this subclade does not contain cultured representatives with lipid data. Scale bars represent the mean number of substitutions per site.

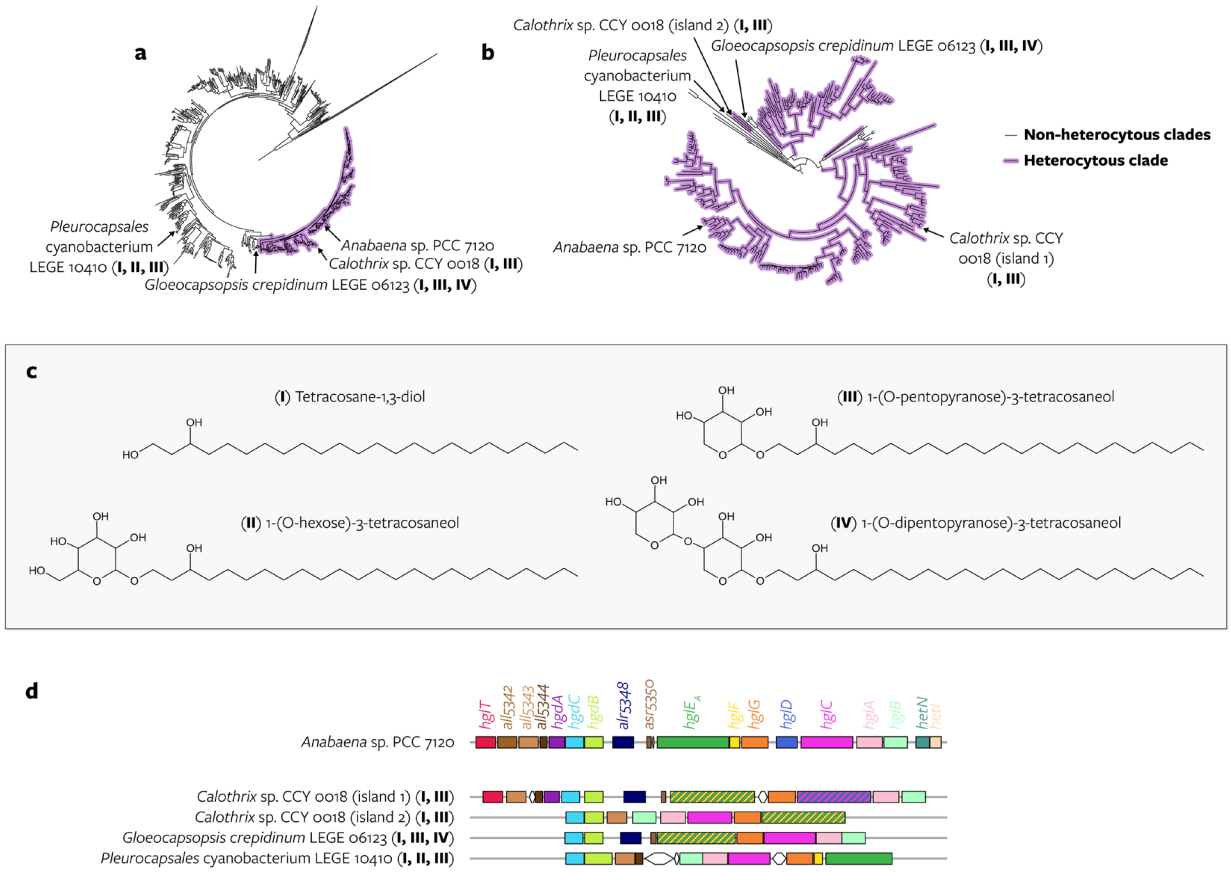

Fig. 6. Two non-heterocytous and one heterocytous cyanobacteria produce HG analogs. a, Position of cyanobacteria that produce HG analogs in the phylogeny based on the concatenated alignment of 24 core vertically-transferred genes (Fig. 2a). The HG analogs that they produce are depicted in panel c and indicated with roman numerals I-IV throughout the figure. *Pleurocapsales* cyanobacterium LEGE 10410 and *Gloeocapsopsis crepidinum* LEGE 06123 are the only non-heterocytous cyanobacteria whose lipids were analyzed. *Anabaena* sp. PCC 7120 does not produce HG analogs but is indicated for reference. **b**, Position of the *hgl* islands of the same cyanobacteria in the concatenated alignment of homologous sequences of 7 HG biosynthesis genes (Fig. 4). Both *hgl* islands of *Calothrix* sp. CCY 0018 are indicated. **c**, Tentative structure of HG analogs. **d**, *Hgl* islands encoded on the genomes of *Anabaena* sp. PCC 7120 and the three cyanobacteria that produce HG analogs.

Online Methods

Bacterial strains and growth conditions

Most cyanobacterial biomass from heterocytous strains was obtained from frozen (-80 °C) culture pellets stored in the former Culture Collection Yerseke (CCY), and from starter cultures provided by the Pasteur Culture Collection (PCC) (Supplementary Tables 1 and 2). The exceptions were *Umezakia ovalisporum* strains UAM290[47] and UAM292 (formerly known as *Chrysosporum ovalisporum* or *Aphanizomenon ovalisporum*), kindly provided by Dr. Samuel Cirés, and *Anabaena* sp. PCC 7120 *wild type* (*wt*) and Δ*hglT*[15], kindly provided by Dr. Koichiro Awai. Non-heterocytous strains were kindly provided by the Blue Biotechnology and Ecotoxicology Culture Collection (LEGE-CC)[48].

Escherichia coli strains NEB® 5-alpha (New England Biolabs) and TOP10 (ThermoFisher Scientific) were used for plasmid manipulation, grown at 37 °C in LB (Miller) Broth (Sigma Aldrich, St. Louis, MO, USA) or in solid LB (Miller) supplemented with bacteriological agar (VWR, Solon, OH, USA). pRL443 (Addgene plasmid # 70261 ; http://n2t.net/addgene:70261; RRID:Addgene_70261) and pRL623 (Addgene plasmid # 58494 ; http://n2t.net/addgene:58494; RRID:Addgene_58494) were a gift from Peter Wolk, and pAM5404 was a gift from Susan Golden (Addgene plasmid # 132660; http://n2t.net/addgene:132660 ; RRID:Addgene_132660) obtained through Addgene (Watertown, MA, USA).

Anabaena sp. PCC 7120 *wild-type (wt)* and Δ*hglT*[15] were routinely grown at 30 °C in liquid BG11 medium or BG11 without nitrogen ($BG11_0$)[46] (see Supplementary Table 2), supplemented with appropriate antibiotics, and incubated under constant white light illumination (60-70 $\mu E/m^2/s$) with or without agitation at 120 rpm (INFORS, Bottmingen, Switzerland). Cells were also grown in solid BG11 medium supplemented with bacteriological agar (VWR, Solon, OH, USA) and the appropriate antibiotics. When required, the following antibiotic concentrations were used: ampicillin (100 µg/ml), kanamycin (20 µg/ml), spectinomycin (25 µg/ml), streptomycin (10 µg/ml), and chloramphenicol (25 µg/ml). Growth of *Anabaena* strains was monitored by measuring OD_{730} in a V-1200 Spectrophotometer (VWR International Europe,

454 Leuven, Belgium). To induce heterocyte formation, cells were either grown directly in $BG11_0$ media or
455 transferred from BG11 to $BG11_0$ by either: (1) washing the culture three times with $BG11_0$ (*wt* and Δ*hglT*)
456 (2) a minimum of five successive 1:10 culture dilutions in $BG11_0$ (ARP001 and ARP003), (3) two to five
457 rounds of cell collection and transfer to $BG11_0$ medium (ARP002n, ARP004-007).

458 *Gloeocapsopsis crepidinum* LEGE 06123 and *Pleurocapsales* cyanobacterium LEGE 10410 were routinely
459 grown at 21 °C in MN and MN_0 media (see Supplementary Table 2) and incubated under a 12:12 light:dark
460 regime, with white light illumination (30-40 $\mu E/m^2/s$) and without agitation (SANYO MLR-350, Japan).
461 Cultures were either grown directly in MN media or transferred from MN to MN_0 using a 1:10 dilution.
462 After three successive transfers in MN_0, cultures were incubated for 38 days and then harvested. To evaluate
463 the effect of other stressors such as nutrient limitation and culture age, the first transfer of the cultures was
464 also harvested after 77 days.

465 Biomass was harvested by centrifugation at 2500 rpm for 10 min, washed 3 times with bi-distilled water
466 and stored at -20 °C until further processing.

467 **Microscopic analysis**

468 Prior to harvesting, strains *Gloeocapsopsis crepidinum* LEGE 06123 and *Pleurocapsales* cyanobacterium
469 LEGE 10410 were analyzed under the microscope. To visualize the presence of external polysaccharide a
470 fresh aliquot of each culture was incubated with an equal volume of a 0.5% solution of Alcian blue (Sigma
471 Aldrich, Steinheim, Germany) at room temperature for 10 min, which was then visualized using bright field
472 microscopy (Axio Imager M2, Zeiss, magnification x200 - x400). Cell lipids were visualized using Nile
473 Red (Sigma Aldrich, Steinheim, Germany), in brief, 40 µl of culture were incubated with 50 µl DMSO 40%
474 and 10 µl Nile Red (10 µlg/ µl in 40% DMSO) at room temperature for 5 to 15 min. Stained samples were
475 then visualized using epifluorescence microscopy on an Axio Imager M2 microscope (Zeiss, magnification
476 x400) coupled to a Colibri LED light source (Zeiss, 555 nm excitation wavelength).

477 **Nucleic acids extraction and sequencing**

478 Genomic DNA (gDNA) was extracted from strains described in Supplementary Table 2 using the DNeasy
479 PowerSoil kit (Qiagen, Hilden, Germany) with minor modifications, namely: samples were disrupted using
480 the bead mill homogenizer ran twice for 10 seconds at a speed of 3.55 m s^{-1} with a 30 second dwell.
481 Concentration of genomic gDNA extracts was analyzed using a Nanodrop ND-1000 Spectrophotometer
482 (NanoDrop Technologies Inc. Wilmington, DE, USA). gDNA was sequenced using Illumina sequencing
483 platform 150bp paired-end, achieving total of 13 to 22 million reads per strain. Library preparation using
484 Illumina TruSeq Nano (350bp insert) library kit and sequencing were carried out by Macrogen Europe
485 (Amsterdam, The Netherlands), whilst library preparation using Nextera XT DNA Library Preparation Kit
486 (96 samples) and sequencing were carried out by Macrogen Korea (Seoul, Republic of Korea)
487 (Supplementary Table 4).

488 **Genome assemblies**

489 Adapter sequences and polyG tails were removed from Illumina reads using Trimmomatic (v0.36; using
490 arguments 'PE', '-phred33', and 'ILLUMINACLIP: adapters.fa:2:30:10 LEADING:20 TRAILING:20
491 SLIDINGWINDOW:5:20 MINLEN:40')[49] and Cutadapt (v1.16; using arguments '--nextseq-trim=20', '-m
492 40', '-q 20', '-n 5', '--discard-trimmed')[50], respectively. Sequence quality was checked using FastQC
493 (v0.11.9)[51]. Sequencing reads were assembled into draft genomes using BiosyntheticSPAdes (v3.14.1)[52].
494 Quality and potential contamination of the assemblies were assessed with BlobTools2 (v2.3.3)[53] integrating
495 the output of BLASTN (v2.10.1+)[54,55] to NCBI nt downloaded on April 1st 2021, DIAMOND blastx
496 (v2.0.8.146)[56] to UniProt 2021_01 database[57], Minimap2 (v2.17-r941)[58] to map the reads back to the
497 assembly and BUSCO (v5.1.1)[59] with database version odb10 . Only contiguous sequences (contigs)
498 assigned as 'Cyanobacteria', not assigned to any phylum ('no-hit'), and to 'Bacterial-undefined' were
499 retained. To confirm the absence of contigs of other phyla in our assemblies we used BlobTools2 integrating
500 data of BLASTN, Minimap2 and BUSCO. This procedure was repeated for four genomes (CCY 9926,
501 CCY 0103, UAM 290 and UAM 292) where proteobacterial contigs had been detected. Additionally in two

502 of these genomes (UAM290 and UAM292) only contigs with a minimum coverage of 3x and a GC
503 percentage of 30-50% were retained.

504 **Selection of publicly available cyanobacterial genome sequences**

505 We downloaded all genomes from the PATRIC genome database[60] (currently part of the BV-BRC
506 database[61]) that had a taxonomic assignment as 'phylum *Cyanobacteria*' (taxonomy ID 1117 according to
507 NCBI taxonomy) based on the 'genome_lineage' file on the PATRIC ftp server (ftp.patricbrc.org) from
508 April 30, 2022. As some of the genome sequences in PATRIC were identical, we identified replicates based
509 on concatenated DNA sequences and concatenated sorted DNA sequences and kept one genome per group
510 of replicates.

511 The final selection of 3,657 genomes (Supplementary Data 1) included 258 genomes with genome status
512 'complete', 3,021 with genome status 'WGS', 342 with genome status 'Plasmid' and 36 with unknown
513 genome status. The genomes were taxonomically reannotated with GTDB-Tk (v2.1.0)[62] using
514 release207_v2 of the Genome Taxonomy Database (GTDB)[63], revealing that most of the chromosomal
515 genomes were from the class *Cyanobacteriia*. The annotation algorithm of GTDB-Tk is based on
516 phylogenetic placement of core genome marker genes and thus does not allow for taxonomic annotation of
517 plasmids. GTDB-Tk placed 52 and 5 genomes in the non-photosynthetic cyanobacterial classes
518 *Vampirovibrionia* and *Sericytochromatia*, respectively, and 20 genomes outside cyanobacteria
519 (Supplementary Data 1). Genome quality was assessed with CheckM (v1.1.3)[64] in the lineage-specific
520 workflow (Supplementary Data 1). Genomes from strains with known morphology (unicellular,
521 baeocytous, filamentous, heterocytous, and ramified) based on ref. [31] were identified based on their
522 taxonomy ID.

523 **Query of HG biosynthesis genes and *hgl* island definition**

524 Proteins were predicted on the PATRIC genomes and on the 14 newly sequenced genomes with Prodigal
525 (v2.6.3)[65] in single genome mode. The 19 protein sequences that are encoded by the *hgl* island of *Anabaena*

526 sp. PCC 7120 (see Supplementary Fig. 1) were extracted from the protein files of
527 GCA000009705.1_ASM970v1 on GenBank[66,67] and queried against a single concatenated protein file
528 containing all proteins of the PATRIC genomes and of the 14 newly sequenced genomes with BLASTP
529 (v2.12.0+)[54]. No protein-coding sequences were predicted on 78 PATRIC genomes, which were all
530 plasmids according to the PATRIC metadata table, and the final set of proteins thus encompassed 3,579
531 genomes. Hits with an *e*-value $\leq 1^{e-5}$ and query coverage ≥ 50% were considered homologous.

532 Because of the potential of gene fusions and fissions, we allowed for multiple hits per open reading frame
533 (ORF) if these hits did not overlap substantially. Hits were defined as 'overlapping' if at least one of the
534 hits had ≥ 50% overlap on the subject sequence with another hit. For a group of overlapping hits, the single
535 best hit was chosen according to bit-score. 'Non-overlapping' hits—i.e. hits that had < 50% overlap on the
536 subject sequence with any other hit—where all considered present on the subject sequence. ORFs with hits
537 to HG biosynthesis genes were considered part of a genomic cluster if they were separated by ≤3 ORFs on
538 the contig. For example, the first predicted ORF and the fifth predicted ORF on a contig were considered
539 connected by this definition, but not the first and the sixth unless an ORF in between also contained a hit
540 to an HG biosynthesis gene. An ORF was considered close to a contig edge if it was within 3 ORFs of the
541 edge, for example the fourth ORF on a contig was considered close to the edge but not the fifth. We
542 examined genomic clusters containing homologs of at least 7 of the queried HG biosynthesis genes—i.e. a
543 genomic cluster of ORFs with hits to at least 7 different HG biosynthesis genes irrespective of the number
544 of ORFs on which they were encoded or the copy number of the gene on the cluster—as '*hgl* islands'.

545 **Query of *nif* genes and identification of glycosyltransferases**

546 *Nif* genes and genomic clusters of *nif* genes were defined similar to the HG biosynthesis genes and genomic
547 clusters described above. We queried nitrogenase protein sequences encoded by *nif* genes from *Anabaena*
548 sp. PCC 7120 of GCA000009705.1_ASM970v1 that are part of the nitrogenase gene cluster depicted in
549 Figure 2 of ref. [68]: alr1407 (*nifV1*), asr1408 (*nifZ*), asr1409 (*nifT*), all1433 (*nifW*), all1436 (*nifX*), all1437
550 (*nifN*), all1438 (*nifE*), all1440 (*nifK*), all1454 (*nifD*), all1455 (*nifH*), all1456 (*nifU*), all1457 (*nifS*), alr1459

551 (*xisF*), and all1517 (*nifB*). Overlapping and non-overlapping hits were defined and dealt with as above for
552 the HG biosynthesis genes, as were genomic clusters of ORFs. The length of a *nif* genomic cluster was
553 defined as the number of queried genes with hits on the genomic cluster irrespective of the number of ORFs
554 on which they were encoded or the copy number of the gene on the cluster. We considered genomic clusters
555 containing homologs of at least 5 of the queried *nif* genes '*nif* islands' and an indication of the genomic
556 capability of nitrogen fixation.

557 To identify glycosyl transferases, we annotated the genomes with dbCAN2, using dbCAN HMMdb
558 (v10.0)[69] and hmmscan, with an *e*-value < 1e-15 and coverage > 0.35.

559 **Cyanobacterial core gene phylogeny**

560 We selected the 2,777 genomes that were taxonomically annotated as 'phylum *Cyanobacteria*' according
561 to GTDB-Tk, and had at least a medium-quality draft status according to the minimum information about
562 metagenome-assembled genome (MIMAG) criteria[70] (estimated completeness ≥ 50% and contamination <
563 10%). Similar genomes were identified with dRep (v3.4.0)[71] using the fastANI algorithm and a similarity
564 cut-off of 95% average nucleotide identity (ANI), which has been suggested as species-level boundary[72].

565 The representative genome of each dRep cluster was used for constructing a phylogeny based on core genes.
566 We started with the 27 Clusters of Orthologous Gene (COG) families that showed evidence of being
567 primarily vertically transferred in ref. [42]. For identification of these genes in the genomes, fasta files from
568 the COG 2020 database were downloaded from the NCBI ftp server
569 (ftp.ncbi.nih.gov/pub/COG/COG2020/data/fasta/), and aligned with MAFFT (v7.505)[73] with the '--
570 anysymbol' flag, using the L-INS-i algorithm if the COG family contained ≤ 800 sequences and default
571 parameters otherwise. HMM profiles were constructed with hmmbuild and hmmpress from the HMMER
572 package (v3.2.2)[74]. The representative genomes, with proteins longer than 100.000 amino acids removed,
573 were annotated with the COG database using hmmscan from the HMMER package and an *e*-value < 1e-5.
574 The best hit was selected per protein sequence based on *e*-value. We counted the occurrence of the COG
575 families in each genome and selected the 24 COG families that were present in single-copy in ≥ 75% of the

576 representative genomes as our final set of core genes. Genes that were single-copy in a genome were
577 extracted and aligned with MAFFT using the L-INS-i algorithm. The alignments were trimmed with trimAl
578 (v1.4.rev15)[75] in gappyout mode. If a sequence contained ≥ 50% gaps after trimming, it was removed from
579 the alignment. The aligned sequences were concatenated per genome, filling in gaps when a gene was
580 absent from the alignment—i.e. when it was not present on the genome or present in multiple copies or
581 when it was removed after trimming. We removed the 18 representative genomes whose concatenated
582 alignment was based on <7 genes. The final concatenated alignment contained 1,260 representative
583 genomes (representing 2,758 genomes) and 6,933 amino acids.

584 A phylogenetic tree was constructed with IQ-TREE (v1.2.1)[76], using 1,000 ultrafast bootstraps[77], and model
585 selection[78] based on nuclear models. The best-fit model (LG+R10) was chosen based on the Bayesian
586 Information Criterion (BIC). The phylogenetic tree was visualized and decorated in Interactive Tree of Life
587 (iTOL)[79]. Pruning of the phylogenetic tree for figures that contained a selection of cyanobacteria was also
588 done in iTOL.

589 **Visualization of *hgl* and *nif* islands on core gene phylogeny**

590 The branches of the core gene phylogeny are representative genomes of dRep clusters that sometimes
591 contain multiple genomes. We decorated each branch on the core gene phylogeny with *hgl* and *nif* islands
592 of one selected genome, and the genome that was chosen for this visualization was not always the dRep
593 representative genome that was used to construct the core gene phylogeny. When the dRep cluster contained
594 a genome from a culture with associated lipid data, this genome was chosen. Alternatively, the genome
595 from the dRep cluster that had the most extended *hgl* island in terms of number of queried genes with hits
596 on the island was chosen.

597 The most extended *hgl* island in terms of number queried genes with hits on the island was drawn on the
598 phylogeny. Presence and absence of a *nif* island in a branch of the core gene phylogeny was based on the
599 same selected genome. Drawing direction of the *hgl* islands was based on the orientation of the *hgdC* / *hgdB*
600 pair, or if the island had no hits to both genes of the *hglG* / *hglC* pair. The oriented *hgl* islands were aligned

601 based on their nucleotide position relative to *hgdB* (no offset) or *hglC* (an offset of 10,135 nucleotides
602 because this is the distance between *hgdB* and *hglG* on the genome of *Anabaena* sp. PCC 7120 (BV-BRC
603 genome identifier 103690.50)).

604 **Phylogenies based on 7 *hgl* island genes**

605 We extracted all hits of 7 HG biosynthesis genes—*hgdCB* and *hglE*$_A$*FGCA*—from the 324 *hgl* islands
606 that were drawn on the core gene phylogeny. Only the protein region of the BLASTP hit was extracted, and
607 when an island contained multiple hits, we picked the best hit in terms of bit-score. 69 *hgl* islands did not
608 contain a hit to all 7 genes and were discarded. The protein sequences were aligned with MAFFT using the
609 E-INS-i algorithm, trimmed with trimAl in gappyout mode, and the aligned sequences were concatenated
610 per *hgl* island. A phylogenetic tree was constructed with IQ-TREE, using 1,000 ultrafast bootstraps, and
611 model selection based on nuclear models. The best-fit model (JTTDCMut+F+R8) was chosen based on the
612 BIC. The phylogenetic tree was visualized and decorated in iTOL. Pruning of the tree to generate Fig. 5
613 and Supplementary Figs. 16, and 23 was done in iTOL.

614 In addition, we made a second phylogeny which included the same hits but also incorporated the hits from
615 the *hgl* islands of 4 cyanobacteria that were not drawn on the core gene phylogeny (Fig. 2). These
616 cyanobacteria were chosen because they are non-diazotrophic cyanobacteria from within the heterocytous
617 clade (*Raphidiopsis curvata* NIES-932, *Cylindrospermopsis raciborskii* CENA303, and *Raphidiopsis*
618 *brookii* D9) or because they possess an *hgl* island but without *hglT* homologs (*Cylindrospermopsis*
619 *raciborskii* CYRF; the highest-scoring *hglT* hit anywhere on its genome has a bit-score of 68.6). For these
620 4 genomes, we included *hgl* islands with hits to at least 6 of the queried genes, and reconstructed an
621 alignment and phylogenetic tree as described above, filling in gaps when a gene was absent from the
622 alignment. The best-fit model (JTTDCMut+F+R9) was chosen based on the BIC. The phylogenetic tree
623 was visualized and decorated in iTOL. Pruning of the tree to generate Supplementary Figs. 15 and 17 was
624 done in iTOL.

625 **Cloning strategy and recombinant plasmid construction**

626 Prior to further genetic modifications we confirmed the substitution of *hglT* for the *npt* kanamycin resistance
627 cassette in the Δ*hglT Anabaena* strain via PCR using two different primer sets (Supplementary Fig. 12 and
628 Supplementary Table 12). The presence of a kanamycin resistance cassette in place of *hglT* was analyzed
629 using primers Fw3_Hali14 and Rv2_Hali14_mod [15], which produced the expected 990 bp fragment (data
630 not shown). Whilst deletion of *hglT* in all genome copies of the Δ*hglT Anabaena* mutant strain was
631 determined using primers HR1_hglT_F and HR2_hglT_R, if *hglT* was present a ~1700 bp band would be
632 seen, whist if *hglT* had been successfully replaced by *npt* we would observe a ~2000 bp band
633 (Supplementary Fig. 12). Our results confirmed that *hglT* had been successfully deleted in all genome
634 copies. However, in addition to the expected ~2000 bp band we also observed a smaller (~550 bp) band
635 (data not shown), which might be caused by the partial loss of the *npt* kanamycin cassette (~800 bp) after
636 kanamycin stepdown upon receival of the strain.

637 The PCRs described above were carried out using 1 µl gDNA extracted as described in the Material and
638 Methods in a 25 µl polymerase chain reaction (PCR) containing, 10 µl PCR water, 5 µl Q solution, 2.5 µl
639 Qiagen Buffer, 2 µl dNTPs (0.25 mM), 1.5 µl $MgCl_2$, 1.25 µl forward primer (4 mM), 1.25 µl reverse
640 primer (4 mM), 0.25 µl BSA (20 mg/mL) and 0.125 µl Qiagen *Taq* polymerase. The conditions for the
641 reaction were as follows: a 10' initial denaturation step at 95 °C was followed by 1' at 95 °C, 1' at 55 °C
642 (Fw3_Hali14 and Rv2_Hali14_mod) or 58 °C (HR1_hglT_F and HR2_hglT_R), 2' at 72 °C, these steps
643 were repeated 30 times, and were followed by a final extension step of 10' at 72 °C.

644 The following genes of interest (GOIs) were selected from the *Richelia intracellularis* HH01 genome (taxon
645 ID 2579778779) and their sequence obtained by using The Integrated Microbial Genomes & Microbiomes
646 system (hereafter IMG/M)[80]: RINTHH_5560, RINTHH_5570, RINTHH_17770 (Ri70) and
647 RINTHH_20790 (Ri84-long). Because RINTHH_5560 and RINTHH_5570 were very closely located, a
648 construct containing both genes and their intergenic region (42bp) (RINTHH_5560_5570) was also
649 included. Additionally, *R. intracellularis* HH01 genome was downloaded and annotated using RAST[81].

650 From this annotation an open reading frame (ORF) annotated as a glycosyltransferase that was highly
651 similar to RINTHH_20790 (Ri84), albeit shorter (39 bp at the 5') was selected. All the aforementioned
652 genes were synthesized by Baseclear BV (Leiden, the Netherlands) under the control of P_{glnA}, a constitutive
653 promoter active in heterocyte and vegetative cells[82].

654 The streptomycin/spectinomycin resistance cassette *aadA*[83], used as selective marker, was also synthesized
655 by Baseclear B.V. and inserted into pBluescript II KS (+). All constructs were flanked by the appropriate
656 GC-adaptors in order to make them compatible for cloning using the CYANO-VECTOR approach[84]. The
657 genes of interest (GOIs) and the resistance cassette were inserted in pAM5404 (Supplementary Fig. 13), an
658 RSF1010-based plasmid containing a mutation in *mobA*Y25F to improve cloning efficiency and an
659 additional RK2-*bom* site to increase its mobilization efficiency[83], as described in ref [84]. In brief, plasmid
660 and inserts were digested using *ZraI I* (New England Biolabs) according to the manufacturer's instructions.
661 Fragments containing the GOIs were purified using a PCR purification kit (QIAquick PCR Purification kit,
662 Qiagen, Hilden, Germany). To remove potential undigested plasmid containing *aadA* in the assembly
663 reaction, the restriction digest of pRP002 was run on a 1% agarose gel, and the appropriate fragment (1279
664 bp) was cut and purified using QIAquick gel extraction kit (Qiagen, Hilden, Germany).

665 Final constructs were assembled using NEBuilder® HiFi DNA Assembly Cloning Kit (New England
666 Biolabs) according to the manufacturer's instructions, transformed into NEB® 5-alpha chemically
667 competent *E. coli* cells and plated on LB agar plates containing spectinomycin and streptomycin. The
668 resulting plasmids were extracted using QIAprep Spin Miniprep Kit (Qiagen, Hilden, Germany) and the
669 presence of the correct insert was confirmed by Sanger sequencing (Baseclear B.V, Leiden, The
670 Netherlands) using the primers PaadA_out, PglnA_F and GOI_R (Supplementary Table 12). In order to
671 make them suitable for tri-parental mating, plasmids (hereafter referred to as cargo plasmids,
672 Supplementary Fig. 14, Supplementary Table 13) were then subcloned in TOP10 cells (Invitrogen,
673 Carlsbad, CA, USA).

674 **Recombinant plasmid transfer via triparental mating**

675 Genetic modification by triparental mating of *Anabaena* sp. PCC 7120 Δ*hglT* was carried out as described
676 in refs [85,86] with a few modifications. As helper strain, we used an *E.coli* strain containing the helper plasmid
677 pRL623 and the conjugal plasmid pRL443[87], hereafter referred to as helper strain. This strain was generated
678 by biparental mating (see below) of an *E.coli* DH5alphaMCR strain containing pRL623 and a DH5alpha
679 strain containing pRL443. *E.coli* cultures of the helper strain and TOP10 cells strains carrying the cargo
680 plasmids were grown overnight at 37 °C, shaking at 225 rpm (Innova 43, New Brunswick Scientific),
681 diluted 1:20 in LB without antibiotics and then grown for 2.5h at 37 °C shaking at 200 rpm in an Erlenmeyer
682 flask of volume 10 times larger than the volume of the culture. Cells were then harvested by centrifugation
683 for 5 min at 2500 rpm and resuspended gently in 1 mL LB per every 10 mL of initial culture. Cargo and
684 helper plasmid were then mixed in a 1:1 ratio in a total volume of 2 mL, harvested by centrifugation for 5
685 min at 2500 rpm, resuspended in 100 µl LB and incubated at 30 °C for 1 h without agitation. For each
686 mating we harvested 1.8-3.5 mL of an *Anabaena* sp. PCC 7120 Δ*hglT* (OD_{730} 0.25-0.5) culture grown in
687 BG11 media plus kanamycin by centrifugation for 5 min at 2500 rpm and resuspended it in 100 µl BG11.
688 *Anabaena* cell concentrates were then mixed with the biparental mating of the *E.coli* strains containing the
689 cargo and helper plasmids, harvested by centrifugation and resuspended in 30 µl BG11. Upon resuspension,
690 cells were plated onto a Supor® Membrane Disc Filter (Pall Laboratories) on BG11 agar plates
691 supplemented with 5% LB. The filters were allowed to dry before incubation at 30°C under light dimmed
692 by covering the plates with a tissue paper. After approximately 24h, the filters were washed with BG11
693 media (Supplementary Table 2) and the resuspended mating's were plated onto BG11 agar plates
694 supplemented with kanamycin, streptomycin and spectinomycin. Upon appearance of *Anabaena* mutant
695 colonies, single colonies were first replated in BG11 agar plates supplemented with antibiotics and then
696 transferred to liquid BG11 media also with appropriate antibiotics. See Supplementary Table 13 for a
697 summary of all the resulting *Anabaena* strains.

698 To check that the desired plasmids had been acquired by the host strain, plasmids were extracted using
699 QIAprep Spin Miniprep Kit (Qiagen, Hilden, Germany) following the manufacturer's instructions with
700 minor modifications, namely: cells from liquid cultures were harvested by centrifugation, resuspended in
701 500 µl P1 and disrupted as previously described (see Materials and Methods). Upon centrifugation the
702 supernatant was processed as described in the manufacturer's protocol. Then the GOI was amplified via 50
703 µl polymerase chain reaction (PCR) containing, 21 µl PCR water, 10 µl Q solution, 5 µl Qiagen Buffer, 4
704 µl dNTPs (0.25 mM), 3 µl $MgCl_2$, 2.5 µl PaadA_out (0.2 mM), 2.5 µl GOI_R (0.2 mM), 0.5 µl BSA (20
705 mg/mL), 0.25 µl Qiagen *Taq* polymerase and 1 µl plasmid DNA. The conditions for the PCR reaction were
706 as follows: a 10' initial denaturation step at 95 °C was followed by 10 cycles of 1' at 95 °C, 1' at 68.4 °C,
707 2' at 72 °C, 20 cycles of 1' at 95 °C, 1' at 67 °C, 2' at 72 °C followed by a final extension step of 10' at
708 72°C.

709 To verify the sequence of the inserted GOIs in the mutant strains, the PCR products of five identical
710 reactions for each strain were pooled and analyzed on a 1% agarose gel. The resulting bands were then
711 purified and concentrated using QIAquick gel extraction kit (Qiagen, Hilden, Germany). The sequences of
712 the concentrated PCR products were confirmed via Sanger sequencing (Baseclear B.V, Leiden, The
713 Netherlands) using the primers PaadA_out, PglnA_F and GOI_R (Supplementary Table 12).

714 **Lipid extraction and analysis**

715 Extraction of intact polar lipids (IPL) from freeze dried biomass was carried out using a modified Bligh
716 Dyer (BD) extraction as described in ref. [88]. A known amount of deuterated
717 diacylglyceryltrimethylhomoserine (DGTS D-9, Avanti® Polar Lipids, USA) dissolved in dichloromethane
718 (DCM) : methanol (MeOH) (1:9, v:v) was added to the extracts as internal standard and then filtered
719 through a true regenerated cellulose 4 mm syringe filter (0.4 µM, BGB, USA). Filtered extracts were
720 analyzed on an Agilent 1290 Infinity I ultra-high performance liquid chromatographer (UHPLC) with a
721 thermostatted auto-injector, coupled to a Q Exactive Orbitrap MS with an Ion Max source and heated
722 electrospray ionization probe (HESI; ThermoFisher Scientific, Waltham, MA) according to ref. [89] (modified

723 from ref [90]). Briefly, chromatographic separation was achieved with an Acquity BEH C18 column (2.1 ×
724 150 mm, 1.7 µm, Waters), with A) MeOH:H_2O:formic acid: (14.8M) NH_3aq (85:15: 0.12:0.04 [v:v]) and
725 B) IPA:MeOH:formic acid:(14.8 M) NH_3aq (50:50:0.12:0.04 [v:v]) at a flow rate of 0.2 mL min^{-1}.
726 Compounds were eluted with 5% B for 3 min, followed by a linear gradient to 40% B at 12 min ending at
727 100% B at 50 min. Lipids were detected using positive ion monitoring of *m/z* 350–2000 (resolution 70,000
728 ppm at *m/z* 200), followed by data dependent MS^2 (isolation window 1 m/z; resolution 17,500 ppm at *m/z*
729 200) of the 10 most abundant ions. HGs were identified using a targeted approach, each sample was
730 screened using the combined molecular mass of the protonated ($[M+H]^+$), ammoniated ($[M+NH_4]^+$) and
731 sodiated ($[M+Na]^+$) adducts and were identified by comparison with published MS^2 spectra (known HGs)
732 and based on theoretical fragmentation for the novel HGs and AGs (extrapolated from the fragmentation of
733 closely related HGs) (Supplementary Table 8).

734 In order to screen for aglycone-like components in the two LEGE strains, their BD extracts were also
735 analyzed by GC-MS after methylation and silyilation. Methylation was carried out using diazomethane
736 (CH_2N_2), then extracts were dried under N_2, cleaned over a small silica gel column (pore size 60 Å, 0.063-
737 0.2mm, 70-230 mesh, Merck), eluted with 3 times the column volume of ethyl acetate (EtAc) and dried
738 under N_2. Silylation was caried out by dissolving the methylated extract in and pyridine (10 µL) and allowed
739 to react with N,O-Bis(trimethylsilyl)trifluoroacetamide (BSTFA, Regis Technologies Inc., IL, USA) at
740 60 °C for 40 min. Samples were then diluted in EtAc and analyzed using a gas chromatographer (Agilent
741 7990B GC) coupled to a mass spectrometer (Agilent 5977A MSD; GC-MS) equipped with a fused silica
742 capillary column (Agilent CP Sil-5, 25 m x 0.32 mm x 0.12 µm). The temperature program was as follows:
743 start at 70 °C, increased to 130 °C at 20 °C min^{-1}, increased to 320 °C at 4 °C min^{-1}, held at 320 °C for
744 25 min. Flow was held constant at 2 mL min^{-1}. For further analysis, some extracts were de-silylated by
745 washing 5 times in DCM (500 µL) and drying under N_2, and then re-silylated by the method above, but
746 with addition of homemade deuterated BSTFA (5 µL) before re-analysis.

747 **Visualization of lipid data on phylogenetic trees**

748 The relative abundances of each HG in relation to the sum of all HGs produced by each strain were plotted
749 as a heatmap on the phylogenetic trees with iTOL. Data from the literature represented with symbols was
750 converted to percentages as follows; “+++”, 90%; “++”, 40%, “+”, 15%; “tr.", 1%.

751 # References

752 1. Zehr, J. P. Nitrogen fixation by marine cyanobacteria. *Trends in Microbiology* **19**, 162–173
753 (2011).

754 2. Martínez-Pérez, C. *et al.* The small unicellular diazotrophic symbiont, UCYN-A, is a key player in
755 the marine nitrogen cycle. *Nat Microbiol* **1**, 1–7 (2016).

756 3. Bentzon-Tilia, M. *et al.* Significant N2 fixation by heterotrophs, photoheterotrophs and
757 heterocystous cyanobacteria in two temperate estuaries. *ISME J* **9**, 273–285 (2015).

758 4. Capone, D. G., Zehr, J. P., Paerl, H. W., Bergman, B. & Carpenter, E. J. Trichodesmium, a Globally
759 Significant Marine Cyanobacterium. *Science* **276**, 1221–1229 (1997).

760 5. Bothe, H., Schmitz, O., Yates, M. G. & Newton, W. E. Nitrogen Fixation and Hydrogen
761 Metabolism in Cyanobacteria. *Microbiol Mol Biol Rev* **74**, 529–551 (2010).

762 6. Awai, K. & Wolk, C. P. Identification of the glycosyl transferase required for synthesis of the
763 principal glycolipid characteristic of heterocysts of Anabaena sp. strain PCC 7120. *FEMS Microbiol Lett*
764 **266**, 98–102 (2007).

765 7. Gambacorta, A., Pagnotta, E., Romano, I., Sodano, G. & Trincone, A. Heterocyst glycolipids from
766 nitrogen-fixing cyanobacteria other than nostocaceae. *Phytochemistry* **48**, 801–805 (1998).

767 8. Wörmer, L., CirÉs, S., VelÁzquez, D., Quesada, A. & Hinrichs, K.-U. Cyanobacterial heterocyst
768 glycolipids in cultures and environmental samples: Diversity and biomarker potential. *Limnol. Oceanogr.*
769 **57**, 1775–1788 (2012).

770 9. Schouten, S. *et al.* Endosymbiotic heterocystous cyanobacteria synthesize different heterocyst
771 glycolipids than free-living heterocystous cyanobacteria. *Phytochemistry* **85**, 115–121 (2013).

772 10. Bale, N. J. *et al.* A novel heterocyst glycolipid detected in a pelagic N2-fixing cyanobacterium of
773 the genus Calothrix. *Organic Geochemistry* **123**, 44–47 (2018).

774 11. Bauersachs, T. Development and application of proxies for past cyanobacterial N_2 fixation.
775 (Faculty of Geosciences Utrecht University, Gologica Ultraiectina No. 327, 2010).

776 12. Pérez Gallego, R., Bale, N. J., Sinninghe Damste, J. S. & Villanueva, L. Developing a genetic
777 approach to target cyanobacterial producers of heterocyte glycolipids in the environment. *Frontiers in*
778 *Microbiology* **14**, (2023).

779 13. Fan, Q. *et al.* Clustered genes required for synthesis and deposition of envelope glycolipids in
780 Anabaena sp. strain PCC 7120: Synthesis of heterocyst envelope glycolipid layer. *Molecular Microbiology*
781 **58**, 227–243 (2005).

782 14. Saito, T. & Awai, K. A polyketide synthase HglEA, but not HglE2, synthesizes heterocyst specific
783 glycolipids in Anabaena sp. PCC 7120. *J Gen Appl Microbiol* **66**, 99–105 (2020).

784 15. Halimatul, H. S. M., Ehira, S. & Awai, K. Fatty alcohols can complement functions of heterocyst
785 specific glycolipids in Anabaena sp. PCC 7120. *Biochemical and Biophysical Research Communications*
786 **450**, 178–183 (2014).

787 16. Bauersachs, T. *et al.* Distribution of long chain heterocyst glycolipids in cultures of the
788 thermophilic cyanobacterium Mastigocladus laminosus and a hot spring microbial mat. *Organic*
789 *Geochemistry* **56**, 19–24 (2013).

790 17. Schaefer, B. *et al.* Microbial life in the nascent Chicxulub crater. *Geology* **48**, 328–332 (2020).

791 18. Bauersachs, T. *et al.* Distribution of heterocyst glycolipids in cyanobacteria. *Phytochemistry* **70**,
792 2034–2039 (2009).

793 19. Bale, N. J. *et al.* Long chain glycolipids with pentose head groups as biomarkers for marine
794 endosymbiotic heterocystous cyanobacteria. *Organic Geochemistry* **81**, 1–7 (2015).

795 20. Bauersachs, T., Russell, J. M., Evans, T. W., Schwalb, A. & Schwark, L. A heterocyte glycolipid-
796 based calibration to reconstruct past continental climate change. *Nat Commun* **12**, 2406 (2021).

797 21. Tomitani, A., Knoll, A. H., Cavanaugh, C. M. & Ohno, T. The evolutionary diversification of
798 cyanobacteria: Molecular–phylogenetic and paleontological perspectives. *Proc Natl Acad Sci U S A* **103**,
799 5442–5447 (2006).

800 22. Hammerschmidt, K., Landan, G., Domingues Kümmel Tria, F., Alcorta, J. & Dagan, T. The Order of
801 Trait Emergence in the Evolution of Cyanobacterial Multicellularity. *Genome Biology and Evolution* **13**,
802 evaa249 (2021).

803 23. Chen, M.-Y. *et al.* Phylogenomics Uncovers Evolutionary Trajectory of Nitrogen Fixation in
804 Cyanobacteria. *Molecular Biology and Evolution* **39**, msac171 (2022).

805 24. Lyons, T. W., Reinhard, C. T. & Planavsky, N. J. The rise of oxygen in Earth's early ocean and
806 atmosphere. *Nature* **506**, 307–315 (2014).

807 25. Wolk, C. P., Ernst, A. & Elhai, J. Heterocyst Metabolism and Development. in *The Molecular*
808 *Biology of Cyanobacteria* (ed. Bryant, D. A.) 769–823 (Springer Netherlands, Dordrecht, 1994).
809 doi:10.1007/978-94-011-0227-8_27.

810 26. Kaplan-Levy, R. N., Hadas, O., Summers, M. L., Rücker, J. & Sukenik, A. Akinetes: Dormant Cells
811 of Cyanobacteria. in *Dormancy and Resistance in Harsh Environments* (eds. Lubzens, E., Cerda, J. & Clark,
812 M.) 5–27 (Springer, Berlin, Heidelberg, 2010). doi:10.1007/978-3-642-12422-8_2.

813 27. Olson, R. D. *et al.* Introducing the Bacterial and Viral Bioinformatics Resource Center (BV-BRC): a
814 resource combining PATRIC, IRD and ViPR. *Nucleic Acids Research* **51**, D678–D689 (2023).

815 28. Ehira, S., Ohmori, M. & Sato, N. Genome-wide Expression Analysis of the Responses to Nitrogen
816 Deprivation in the Heterocyst-forming Cyanobacterium Anabaena sp. Strain PCC 7120. *DNA Research* **10**,
817 97–113 (2003).

818 29. Shvarev, D., Nishi, C. N., Wörmer, L. & Maldener, I. The ABC Transporter Components HgdB and
819 HgdC are Important for Glycolipid Layer Composition and Function of Heterocysts in Anabaena sp. PCC
820 7120. *Life (Basel)* **8**, 26 (2018).

821 30. Shvarev, D., Nishi, C. N. & Maldener, I. Glycolipid composition of the heterocyst envelope of
822 Anabaena sp. PCC 7120 is crucial for diazotrophic growth and relies on the UDP-galactose 4-epimerase
823 HgdA. *MicrobiologyOpen* **8**, e00811 (2019).

824 31. Shih, P. M. *et al.* Improving the coverage of the cyanobacterial phylum using diversity-driven
825 genome sequencing. *Proc. Natl. Acad. Sci. U.S.A.* **110**, 1053–1058 (2013).

826 32. Black, T. A. & Wolk, C. P. Analysis of a Het- mutation in Anabaena sp. strain PCC 7120 implicates
827 a secondary metabolite in the regulation of heterocyst spacing. *J Bacteriol* **176**, 2282–2292 (1994).

828 33. Bauer, C. C. *et al.* Suppression of heterocyst differentiation in Anabaena PCC 7120 by a cosmid
829 carrying wild-type genes encoding enzymes for fatty acid synthesis. *FEMS Microbiology Letters* **151**, 23–
830 30 (1997).

831 34. Callahan, S. M. & Buikema, W. J. The role of HetN in maintenance of the heterocyst pattern in
832 Anabaena sp. PCC 7120. *Molecular Microbiology* **40**, 941–950 (2001).

833 35. Montejano, G., Becerra-Absalón, I., Gold-Morgan, M. & Osorio-Santos, K. Gloeobacter violaceus:
834 primitive reproductive scheme and its significance. *Plant Syst Evol* **304**, 1221–1229 (2018).

835 36. Rippka, R., Waterbury, J. & Cohen-Bazire, G. A cyanobacterium which lacks thylakoids. *Arch.*
836 *Microbiol.* **100**, 419–436 (1974).

837 37. Awai, K., Lechno-Yossef, S. & Wolk, C. P. Heterocyst Envelope Glycolipids. in *Lipids in*
838 *Photosynthesis: Essential and Regulatory Functions* (eds. Wada, H. & Murata, N.) 179–202 (Springer
839 Netherlands, Dordrecht, 2009). doi:10.1007/978-90-481-2863-1_9.

840 38. Abreu, V. A. C. *et al.* Genomic and Genotypic Characterization of Cylindrospermopsis raciborskii:
841 Toward an Intraspecific Phylogenetic Evaluation by Comparative Genomics. *Front Microbiol* **9**, 306
842 (2018).

843 39. Soriente, A. *et al.* Heterocyst glycolipids of the cyanobacterium Cyanospira rippkae.
844 *Phytochemistry* **33**, 393–396 (1993).

845 40. Bauersachs, Gugger, M. & Schwark, L. Heterocyte glycolipid diketones: A novel type of
846 biomarker in the N2-fixing heterocytous cyanobacterium Microchaete sp. *Organic Geochemistry* **141**,
847 103976 (2020).

848 41. Fay, P., Lynn, J. A. & Majer, S. C. Akinete development in the planktonic blue-green alga
849 *Anabaena circinalis*. *British Phycological Journal* **19**, 163–173 (1984).

850 42. Moody, E. R. *et al.* An estimate of the deepest branches of the tree of life from ancient vertically
851 evolving genes. *eLife* **11**, e66695 (2022).

852 43. Soo, R. M. *et al.* An Expanded Genomic Representation of the Phylum Cyanobacteria. *Genome*
853 *Biology and Evolution* **6**, 1031–1045 (2014).

854 44. Soo, R. M., Hemp, J. & Hugenholtz, P. Evolution of photosynthesis and aerobic respiration in the
855 cyanobacteria. *Free Radical Biology and Medicine* **140**, 200–205 (2019).

856 45. Castenholz, R. W. *et al.* Phylum BX. Cyanobacteria. in *Bergey's Manual® of Systematic*
857 *Bacteriology: Volume One : The Archaea and the Deeply Branching and Phototrophic Bacteria* (eds.
858 Boone, D. R., Castenholz, R. W. & Garrity, G. M.) 473–599 (Springer, New York, NY, 2001).
859 doi:10.1007/978-0-387-21609-6_27.

860 46. Rippka, R., Deruelles, J., Waterbury, J. B., Herdman, M. & Stanier, R. Y. Generic Assignments,
861 Strain Histories and Properties of Pure Cultures of Cyanobacteria. *Microbiology,* **111**, 1–61 (1979).

862 47. Wormer, L., Cirés, S., Carrasco, D. & Quesada, A. Cylindrospermopsin is not degraded by co-
863 occurring natural bacterial communities during a 40-day study. *Harmful Algae* **7**, 206–213 (2008).

864 48. Ramos, V. *et al.* Cyanobacterial diversity held in microbial biological resource centers as a
865 biotechnological asset: the case study of the newly established LEGE culture collection. *J Appl Phycol* **30**,
866 1437–1451 (2018).

867 49. Bolger, A. M., Lohse, M. & Usadel, B. Trimmomatic: a flexible trimmer for Illumina sequence
868 data. *Bioinformatics* **30**, 2114–2120 (2014).

869 50. Martin, M. Cutadapt removes adapter sequences from high-throughput sequencing reads.
870 *EMBnet.journal* **17**, 10–12 (2011).

871 51. Andrews, S. FastQC: a quality control tool for high throughput sequence data.
872 https://www.bioinformatics.babraham.ac.uk/projects/fastqc/ (2010).

873 52. Meleshko, D. *et al.* BiosyntheticSPAdes: Reconstructing Biosynthetic Gene Clusters From
874 Assembly Graphs. *Genome Res.* gr.243477.118 (2019) doi:10.1101/gr.243477.118.

875 53. Challis, R., Richards, E., Rajan, J., Cochrane, G. & Blaxter, M. BlobToolKit – Interactive Quality
876 Assessment of Genome Assemblies. *G3 Genes|Genomes|Genetics* **10**, 1361–1374 (2020).

877 54. Altschul, S. F., Gish, W., Miller, W., Myers, E. W. & Lipman, D. J. Basic local alignment search
878 tool. *J Mol Biol* **215**, 403–410 (1990).

879 55. Camacho, C. *et al.* BLAST+: architecture and applications. *BMC Bioinformatics* **10**, 421 (2009).

880 56. Buchfink, B., Xie, C. & Huson, D. H. Fast and sensitive protein alignment using DIAMOND. *Nat*
881 *Methods* **12**, 59–60 (2015).

882 57. The UniProt Consortium. UniProt: the universal protein knowledgebase in 2021. *Nucleic Acids*
883 *Research* **49**, D480–D489 (2021).

884 58. Li, H. Minimap2: pairwise alignment for nucleotide sequences. *Bioinformatics* **34**, 3094–3100
885 (2018).

886 59. Manni, M., Berkeley, M. R., Seppey, M., Simão, F. A. & Zdobnov, E. M. BUSCO Update: Novel and
887 Streamlined Workflows along with Broader and Deeper Phylogenetic Coverage for Scoring of Eukaryotic,
888 Prokaryotic, and Viral Genomes. *Molecular Biology and Evolution* **38**, 4647–4654 (2021).

889 60. Davis, J. J. *et al.* The PATRIC Bioinformatics Resource Center: expanding data and analysis
890 capabilities. *Nucleic Acids Research* **48**, D606–D612 (2020).

891 61. Olson, R. D. *et al.* Introducing the Bacterial and Viral Bioinformatics Resource Center (BV-BRC): a
892 resource combining PATRIC, IRD and ViPR. *Nucleic Acids Res* **51**, D678–D689 (2023).

893 62. Chaumeil, P.-A., Mussig, A. J., Hugenholtz, P. & Parks, D. H. GTDB-Tk v2: memory friendly
894 classification with the genome taxonomy database. *Bioinformatics* **38**, 5315–5316 (2022).

895 63. Parks, D. H. *et al.* GTDB: an ongoing census of bacterial and archaeal diversity through a
896 phylogenetically consistent, rank normalized and complete genome-based taxonomy. *Nucleic Acids*
897 *Research* **50**, D785–D794 (2022).

898 64. Parks, D. H., Imelfort, M., Skennerton, C. T., Hugenholtz, P. & Tyson, G. W. CheckM: assessing
899 the quality of microbial genomes recovered from isolates, single cells, and metagenomes. *Genome Res.*
900 **25**, 1043–1055 (2015).

901 65. Hyatt, D. *et al.* Prodigal: prokaryotic gene recognition and translation initiation site
902 identification. *BMC Bioinformatics* **11**, 119 (2010).

903 66. Kaneko, T. Complete Genomic Sequence of the Filamentous Nitrogen-fixing Cyanobacterium
904 Anabaena sp. Strain PCC 7120. *DNA Research* **8**, 205–213 (2001).

905 67. Sayers, E. W. *et al.* GenBank. *Nucleic Acids Research* **48**, D84–D86 (2020).

906 68. Esteves-Ferreira, A. A. *et al.* Cyanobacterial nitrogenases: phylogenetic diversity, regulation and
907 functional predictions. *Genet Mol Biol* **40**, 261–275 (2017).

908 69. Zhang, H. *et al.* dbCAN2: a meta server for automated carbohydrate-active enzyme annotation.
909 *Nucleic Acids Res* **46**, W95–W101 (2018).

910 70. Bowers, R. M. *et al.* Minimum information about a single amplified genome (MISAG) and a
911 metagenome-assembled genome (MIMAG) of bacteria and archaea. *Nat Biotechnol* **35**, 725–731 (2017).

912 71. Olm, M. R., Brown, C. T., Brooks, B. & Banfield, J. F. dRep: a tool for fast and accurate genomic
913 comparisons that enables improved genome recovery from metagenomes through de-replication. *ISME*
914 *J* **11**, 2864–2868 (2017).

915 72. Olm, M. R. *et al.* Consistent Metagenome-Derived Metrics Verify and Delineate Bacterial Species
916 Boundaries. *mSystems* **5**, 10.1128/msystems.00731-19 (2020).

917 73. Katoh, K. & Standley, D. M. MAFFT Multiple Sequence Alignment Software Version 7:
918 Improvements in Performance and Usability. *Molecular Biology and Evolution* **30**, 772–780 (2013).

919 74. Eddy, S. R. Accelerated Profile HMM Searches. *PLoS Comput Biol* **7**, e1002195 (2011).

920 75. Capella-Gutiérrez, S., Silla-Martínez, J. M. & Gabaldón, T. trimAl: a tool for automated alignment
921 trimming in large-scale phylogenetic analyses. *Bioinformatics* **25**, 1972–1973 (2009).

922 76. Minh, B. Q. *et al.* IQ-TREE 2: New Models and Efficient Methods for Phylogenetic Inference in
923 the Genomic Era. *Mol Biol Evol* **37**, 1530–1534 (2020).

924 77. Hoang, D. T., Chernomor, O., von Haeseler, A., Minh, B. Q. & Vinh, L. S. UFBoot2: Improving the
925 Ultrafast Bootstrap Approximation. *Molecular Biology and Evolution* **35**, 518–522 (2018).

926 78. Kalyaanamoorthy, S., Minh, B. Q., Wong, T. K. F., von Haeseler, A. & Jermiin, L. S. ModelFinder:
927 fast model selection for accurate phylogenetic estimates. *Nat Methods* **14**, 587–589 (2017).

928 79. Letunic, I. & Bork, P. Interactive Tree Of Life (iTOL) v5: an online tool for phylogenetic tree
929 display and annotation. *Nucleic Acids Research* **49**, W293–W296 (2021).

930 80. Chen, I.-M. A. *et al.* The IMG/M data management and analysis system v.6.0: new tools and
931 advanced capabilities. *Nucleic Acids Research* **49**, D751–D763 (2021).

932 81. Aziz, R. K. *et al.* The RAST Server: Rapid Annotations using Subsystems Technology. *BMC*
933 *Genomics* **9**, 75 (2008).

934 82. Elhai, J. & Wolk, C. P. Developmental regulation and spatial pattern of expression of the
935 structural genes for nitrogenase in the cyanobacterium Anabaena. *EMBO J* **9**, 3379–3388 (1990).

936 83. Bishé, B., Taton, A. & Golden, J. W. Modification of RSF1010-Based Broad-Host-Range Plasmids
937 for Improved Conjugation and Cyanobacterial Bioprospecting. 13 (2019).

938 84. Taton, A. *et al.* Broad-host-range vector system for synthetic biology and biotechnology in
939 cyanobacteria. *Nucleic Acids Research* **42**, e136–e136 (2014).

940 85. Elhai, J. & Wolk, C. P. [83] Conjugal transfer of DNA to cyanobacteria. in *Methods in Enzymology*
941 vol. 167 747–754 (Academic Press, 1988).

942 86. Thiel, T. & Peter Wolk, C. [13] Conjugal transfer of plasmids to cyanobacteria. in *Methods in*
943 *Enzymology* vol. 153 232–243 (Academic Press, 1987).

944 87. Elhai, J., Vepritskiy, A., Muro-Pastor, A. M., Flores, E. & Wolk, C. P. Reduction of conjugal transfer
945 efficiency by three restriction activities of Anabaena sp. strain PCC 7120. *Journal of Bacteriology* **179**,
946 1998–2005 (1997).

947 88. Bale, N. J. *et al.* C_5 glycolipids of heterocystous cyanobacteria track symbiont abundance in the
948 diatom *Hemiaulus hauckii* across the tropical North Atlantic. *Biogeosciences* **15**, 1229–1241 (2018).

949 89. Bale, N. J. *et al.* Lipidomics of Environmental Microbial Communities. I: Visualization of
950 Component Distributions Using Untargeted Analysis of High-Resolution Mass Spectrometry Data.
951 *Frontiers in Microbiology* **12**, (2021).

952 90. Wörmer, L., Cires, S., Velazquez, D., Quesada, A. & Hinrichs, K.-U. Cyanobacterial heterocyst
953 glycolipids in cultures and environmental samples: Diversity and biomarker potential. *Limnol. Oceanogr.*
954 **57**, 1775–1788 (2012).